Tool wear monitoring of high-speed broaching process with carbide tools to reduce production errors

A. del Olmo [b],[*], L.N. López de Lacalle [a],[b], G. Martínez de Pissón [b], C. Pérez-Salinas [c], J.A. Ealo [b], L. Sastoque [b], M.H. Fernandes [a]

[a] Dpt. of Mechanical Engineering, University of the Basque Country (UPV/EHU), Plaza Torres Quevedo s/n, 48013 Bilbao, Spain
[b] Advanced Manufacturing Centre for Aeronautics (CFAA), University of the Basque Country (UPV/EHU), Parque Tecnológico de Bizkaia-Ed. 202, 480170 Zamudio, Spain
[c] Dpt. of Materials and Manufacturing, Technical University of Ambato (UTA), Av. Los Chasquis y Rio Payamino s/n, 180207 Ambato, Ecuador

ARTICLE INFO

ABSTRACT

Real-time monitoring in CNC machine tools is focused on the early detection of tool wear, and in this way to assess part piece quality. The machining process known as broaching is critical for firtree slots (dovetails) production in turbomachinery components, such as turbine disks. Tight tolerances on one hand, even less than 5 μm in firtree-slots pressure faces, and high productivity on the other, are the two main requirements. Besides, broaching tools are very expensive and the cutting edges wear must be estimated during the process; in fact, tool wear in difficult-to-cut materials machining may cause a waste not only in terms of the tool but also of the very expensive workpieces. Broaching usually is one of the last operations in the process chain, so components start the operation with a very high-added value. Hence, only one bad slot implies an unrecoverable piece and therefore a huge waste of time and money.

In this paper, a monitoring method for efficient broaching is proposed by combining real-time monitoring and off-line tool wear inspection. Firstly, the cutting tool characteristics are defined, and those affected by tool degradation. Secondly, some broaching cycles were carried out while measuring a) process accelerations through two accelerometers, b) cutting force by load cells, and c) motor drive consumption. They were simultaneously recorded. Furthermore, the sensitivity between tool wear and broaching process natural frequencies is established.

Finally, a series of experimental tests were executed for verification, showing the useful approach for daily life production. The paper focuses on signals and their sensitivity to significant process variations.

1. Introduction

Broaching is widely used in the manufacturing of parts of complex internal and external profiles, with tight dimensional requirements (IT6/IT7) and requirements for high surface integrity (Ra = 0,8 μm), as well as high repeatability [1]. It is considered the

Nomenclature

|	
SL	Supervised learning
IT	International Tolerance (ISO quality grades)
WEDM	Wire Electrical Diskharge Machining
HSS	High Speed Steel
FEM	Finite Element Method
PLC	Programmable Logic Controller
5G	Fifth generation telecommunications technologies
ACS	Accelerometer coordinate system
MCS	Machine coordinate system
Z	Tool edge number
Ze	Number of teeth engaged into workpiece
A(B1), B(B2), C(B3)	Machining Broach segments A,B,C
Acc1, Acc2	Accelerometers 1,2
VBa	Average flank wear land width
Ra	Average Roughness [μm]
MRR	Material Remove Rate[%]
Vc	Cutting speed [m/s]
b	Tooth width [mm]
e	Thickness of the workpiece [mm]
h	Rise per tooth [μm]
P	Pitch per tooth [mm]
L	Land [mm]
H	Tooth heigh [mm]
r_1, r_2	Gullet round [mm]
r_β	Edge radius [mm]
α	Relief angle [°]
γ	Rake angle [°]
T_{pf}	Tooth passing frequency [Hz]
Fc	Cutting force [N]
X	Adjustment coefficient [adimensional]
Ks	Specific cutting force parameter [N/mm2]
fs	Harmonic frequencies [Hz]
N_{fs}	Number of harmonics
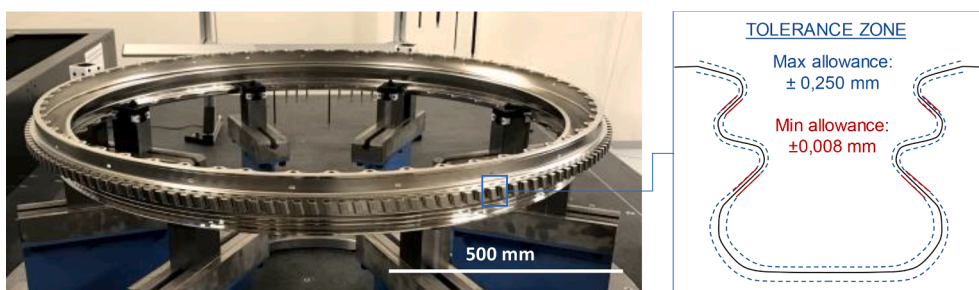
Fig. 1. Left) Low-pressure turbine disk. Right) typical tolerances of slot profile.

"first choice" because it has several advantages over other processes. One outstanding one is that roughing and finishing can be completed in only one machine stroke, which otherwise would require many passes with other machining operations such as milling. In addition, the linear straight and non-rotating tool movement results in very good surface finishing. It is particularly applicable in the manufacture of aero-engine disks. Thus, in Fig. 1 a turbine disk is presented, including around 100 to 160 slots per disk, usually with a firtree shape.

However, achieving high quality and productivity in real production requires a well-supervised operation, focusing on the broaching tool state. Broaching tool condition has a significant influence on achieving the level of surface integrity required for aircraft engine components [2]. However, due to the high-strength and corrosion resistance associated with superalloys, such as Inconel 718, Waspaloy, Rene 104 and IN100 PM, the wear of cutting tools increases rapidly, until tools must be replaced or/and resharpened. Tool
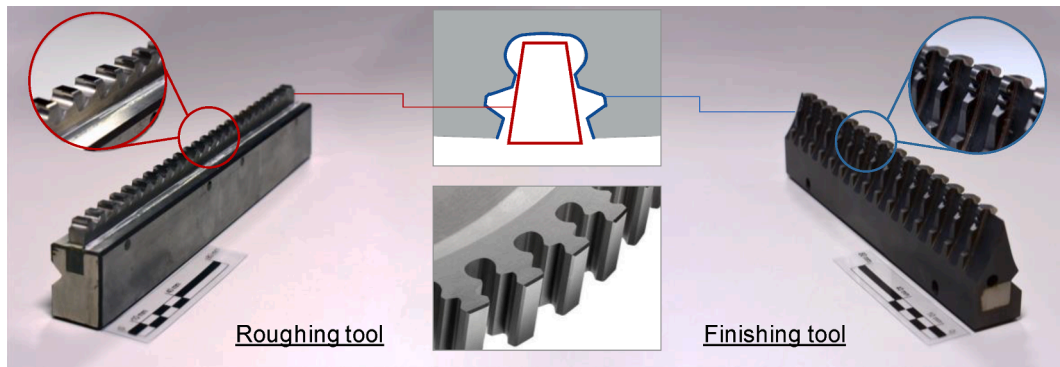
Fig. 2. Roughing (rectangular-trapezoidal) and finishing (firtree) external broaching tools for turbine disks.

wear is caused by thermal fracturing, attrition, abrasion, plastic deformation, diffusion and substrate grains pull-out. So, working with worn tools affects a) the dimensional accuracy, b) surface quality of finished components, and c) even process stability (vibrations) will deteriorate. Consequently, for quality and productivity improvement, a tool wear monitoring system is well recommended in super alloys machining. So, by a correct tool wear monitoring system, tool worm rate can be accurately determined and tool replaced in time to avoid the "scrapping" of critical components; each component is worth several hundreds of thousands of euros/dollars and two or three pieces saved can pay off all the monitoring investment. Furthermore, with an accurate enough wear prediction, broaching tool regrinding will be cost-effective, and tool life can be prolonged significantly.

The first mention of broaching dates back to the 19th century [3]. Despite the advantages it offers [4], documentation about broaching is scarce. In broaching through only one linear movement the designed groove/slot profile is obtained. The broaching tool consists of a shaft (in cylindrical tools) or a long plate (in linear tools) where several teeth with progressive heights (or shifts) are set in growing order, one after the other, in a row. The sum of all consecutive cuts achieves the slot final shape. Different broaching tools for turbines are shown in Fig. 2. Rectangular-trapezoidal shaped ones are for roughing, whereas the finishing ones are firtree shaped. Trapezoidal shapes are near to rectangle profiles. A broaching tool set usually includes 5–8 segments for roughing and 4–6 segments for finishing.

Early publications focused on explaining the broaching fundamentals and the issues related to accuracy and machined surface quality [5,6]. Hence, the evaluation of broaching process accuracy due to the influence of tool and workpiece deflection was disclosed for external [5], as well as, for internal broaching [6], which in the latter the burnishing effect caused by worm tools [7] that increases with workpiece thickness is discussed. Tool design is probably the most critical step, since in broaching all the process parameters, except cutting speed, are contained in the tool geometry itself. However, due to broaching productivity compared to other cutting strategies [8], such as WEDM, the high cost of broaching tools is assumed. Even so, many works still focused on the design of the broaching tools to improve this technology [2,9-11]. The influence of each process parameter like cutting speed, tool cutting angles, or tool material on surface roughness were studied for external [2] as well as for internal broaching [9]. Other studies based on cutting performance optimization, discussed how to improve Material Remove Rate (MRR), or how to improve broaching tool design [10,11]. Besides tool geometry, tool constitutive material is utterly important. Some studies proposed carbon-free cutting materials to replace high-speed steel (HHS), which introduces a higher hot hardness and increased thermal conductivity [12], likewise sintered carbide for roughing tools, which lead to higher process performances [13].

New research had gone one step further, using mathematical algorithms and mechanical models to enhance the broaching tool design. The prediction of cutting forces through the combination of cutting force models based on FE-simulation of chip formation showed good results in [14,15], reducing the amount of experimentation in roughing operations. However, when comes to more complex geometries, such as firtree-shaped finishing tools, cutting force models are usually based on cutting edge discretization [16]. Some investigations developed thermo-mechanical models to predict cutting forces [17]. Even though force modeling software helps the design of broaching tools and to keep the cutting forces in a controllable range, monitoring will always be necessary to detect process disturbances [2]. Broaching is a one-parameter process, i.e., cutting speed, all the others are defined in tool geometry, therefore, a good tool state will imply a stable manufacturing process.

The literature includes many studies concerning signal analysis and tool condition monitoring for turning, milling, grinding and drilling processes. Nonetheless, despite the elevated cost of broaching tools, little attention has been paid to broaching monitoring. During broaching process, tool wear continuously grows and so cutting force does. So some research aimed at establishing a relationship between cutting force and tool wear, installing piezoelectric force sensors in the machine to obtain an approximated tool wear value [18]. The usual tool condition monitoring approach is based on full-equipped machines with different sensors to find a proper correlation between tool condition and process output signals. Different types of sensors can be used, such as vibration transducers (for example, piezoelectric accelerometers), acoustic emission sensors, load cells, thermocouples, etc. The advantages and disadvantages of different broaching monitoring approaches are summarised in [19]. So, in Table 1 the most relevant conclusions are exposed, for a hydraulically driven machine.

The detection of surface anomalies in broaching was successfully extended to identify and locate those related to part quality, such

Table 1
Summary of sensor effectiveness in detecting broaching tool condition [19].

Tool Condition	Output signals [1]			
	Cutting forces	Acoustic emission	Vibrations	Hydraulic pressure
Chipped tooth	🟢	🔴, 🟢/🔺		
Weakened tooth	🟢	🔴, 🔺	🟢, 🔺	
Broken tooth	🟢	🟢	🟢	🟢
Worn teeth	🟢	🟢, 🔺	🟢, 🔺	🟢

Time-domain: (🟢) high effectiveness; (🔴) reduced effectiveness.
Frequency domain: (🔺) high effectiveness; (🔺) reduced effectiveness.
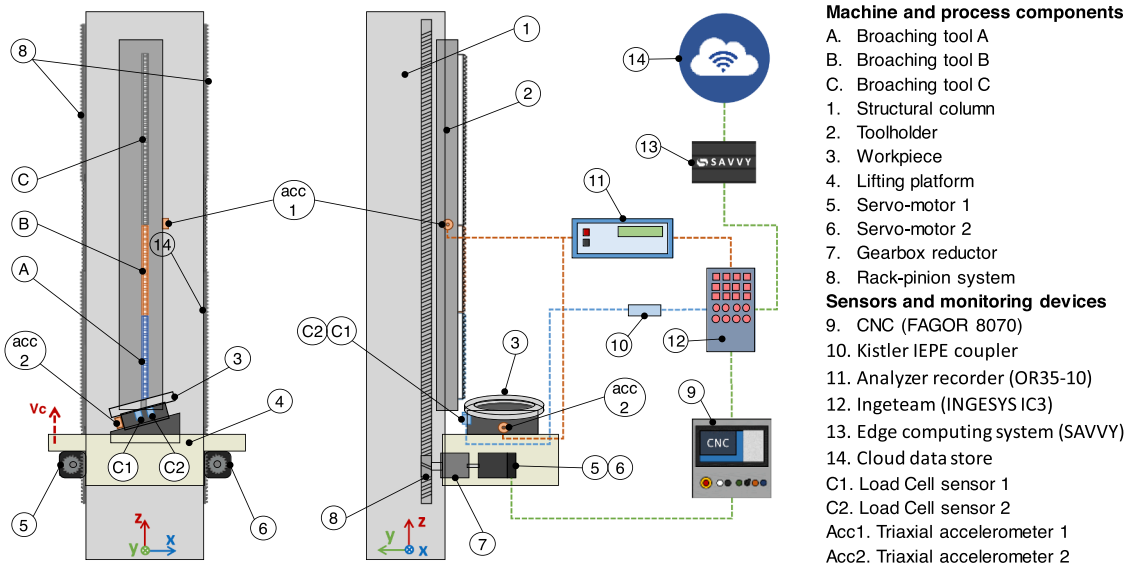
Fig. 3. Data acquisitions system architecture, which position of components, sensors devices of edge computing devices. Motor and rack pinion are twin, placed at both sides of the column.

as scoring, smearing and surface heat-affected zones, based on the analysis of acoustic emission and force signals in the frequency domain [20]. As the broaching process is relatively slow, with only one degree of freedom, monitoring based on strain gauges was also studied [21]. Thus, aeroengine manufacturers are concerned about safety, surface integrity, and the possibility of surface anomalies. Consequently, accurate tool wear monitoring systems is a current necessity [22], tool wear rate can be accurately estimated and therefore tools can be replaced in time to avoid damage to critical components. Furthermore, with an accurate enough prediction, broaching tool regrinding will be cost-effective and tool life can be significantly extended.

This paper aims to propose a tool wear monitoring procedure using a fully-equipped sensor broaching machine. The organization of the work is as follows. Firstly, the monitoring system and the broaching machine are described. Secondly, some examples of tool condition monitoring are given. Then, data analysis is done to extract relevant features. This will allow finding a correlation between tool wear rate and sensor signals. Finally, the broaching experimental results, data from the proposed monitoring system, and the discussion of the results are presented.

2. Tool condition monitoring system

An experimental arrangement was prepared to record process vibrations, forces, as well as machine signals during the external broaching operation of aero-engine low-pressure turbine disks.
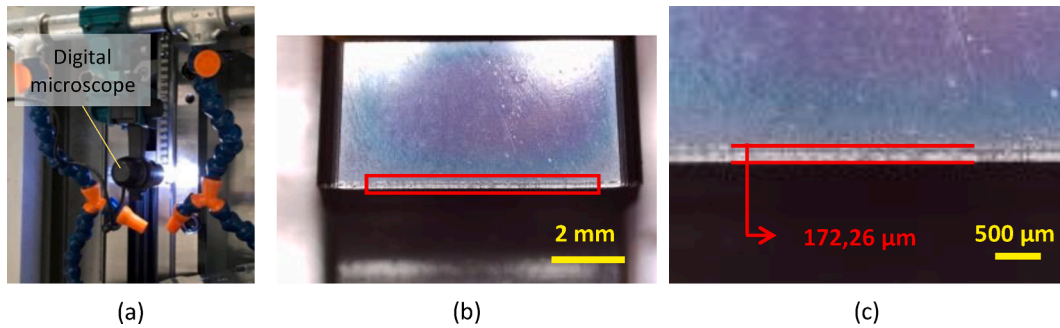
Fig. 4. The (a) In situ tool wear acquisition system by an optical camera **(b)** Broaching tool tooth with flank wear **(c)** Flank wear VB measurement during broaching cycle.

Table 2
Inconel 718 composition and mechanical properties (in aged condition) [23,24].

Ni	Cr	Co	Fe	Nb	Mo	Ti	Al	B	C	Mn	Si	Other
52,5	19	1	17	5	3	1	0.6	0.01	0.08	0,35	0,35	1,79

Hardness	Young's Modulus	Tensile Strength	Density	Specific Heat	Melting Temperature	Thermal Conductivity
42 HRC	206 GPa	1,73 GPa	8470 kg/m^3	461 J/(kg·K)	1550 K	15 W/(m·K)

2.1. System setup

The architecture of the tool wear monitoring system, and the full-equipped broaching machine, are shown in Fig. 3. Here, the electromechanical vertical broaching machine (Ekin® A218/ RASHEM) is shown. In this new machine, broaching tool segments remain static into the machine column, while the piece is bolted on a rotary table that will be moved vertically along the column (broaching/cutting is in the up-stroke), driven by two integrated servo-motors using *a rack and pinion* mechanism, in a twin scheme (twin motors are labels 5 and 6). The opposite is perhaps more usual in the industry, i.e., workpiece disk is fixed meanwhile tool moves, exactly the reverse relative movement. On the other hand, traditional industrial machines are hydraulically powered. The used one was electrically driven, and higher cutting speeds than hydraulic-powered broaching machines are achieved, until a maximum of 40 m/min. The use of electro-driven machines is an increasing trend in the market, and it is expected to spread in many industrial sectors in the non-distant future. The machine includes a coolant system with pump and 4 nozzles to deliver flood coolant (straight oil is the most common) (Fig. 4).

Thus, in Fig. 3 various sensors are shown. Miniature integrated cell force sensors and accelerometers were employed. Additionally, the two servo-motors were the source of more information, by reading the motor drivers using a data-logger Fagor® software program. From the motor drivers, much information was obtained: torque feedback, power consumption, active power consumption, electrical current feedback, temperature, and rotation speed. In addition, the real feed speed, and real linear acceleration of the two electric AC motors were acquired at a sampling rate of 250 Hz (explained later).

On the other hand, the acceleration and force signals were acquired using piezoelectric triaxial accelerometers (PCB™ 604B31) and load cell sensors (PCB™ 208C05) respectively, connected to a modular multi-analyzer/recorder instrument OR35-10 channels system. OR35-10 channels system. All acceleration signals were sampled at 12,800 Hz, while force measurements were acquired at 51,200 Hz. In all the cases, the response frequency was compared against the tooth passing frequency during the broaching process. The sensors resonant frequencies were avoided. All the signal analyses were carried out on an edge-computing device (Ingeteam™) to identify irregular patterns in output signals. The *start and stop times* were established by the edge computing device (Savvy™) by reading machine PLC, and in this way triggering all measurements devices at the same time.

Through a digital microscope (PCE©-MM 200UV) mounted on the machine itself, it was possible to take a photo of each of the broaching tool teeth, without the need to remove tool from the machine (impossible because tool setup is very complex). The purpose was to measure all teeth wear and photo recording was carried out every 5 slots produced, thanks to the short time needed to get and process the images.

Once the entire disk was broached all around, a quality inspection was carried out to determine a) the correct geometry of each slot, b) the roughness at several slot faces, and c) in the broaching tool, the teeth final state.

The machine can be connected wirelessly by a 5G in-door network, but this does not affect the proposed idea; it is only a good example of how current connectivity advances can help to manufacture.

2.2. Broaching tool and parameters

Workpiece was made of nickel-base alloy, Inconel 718, a very common material employed on aero-engine components. Inconel 718
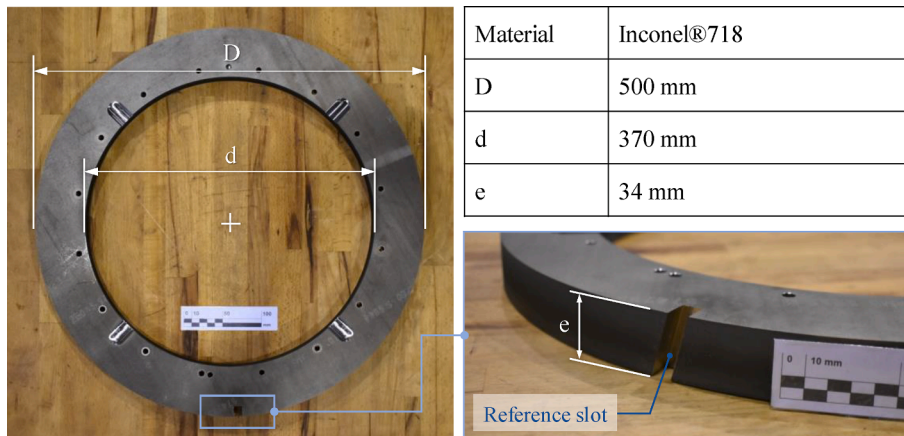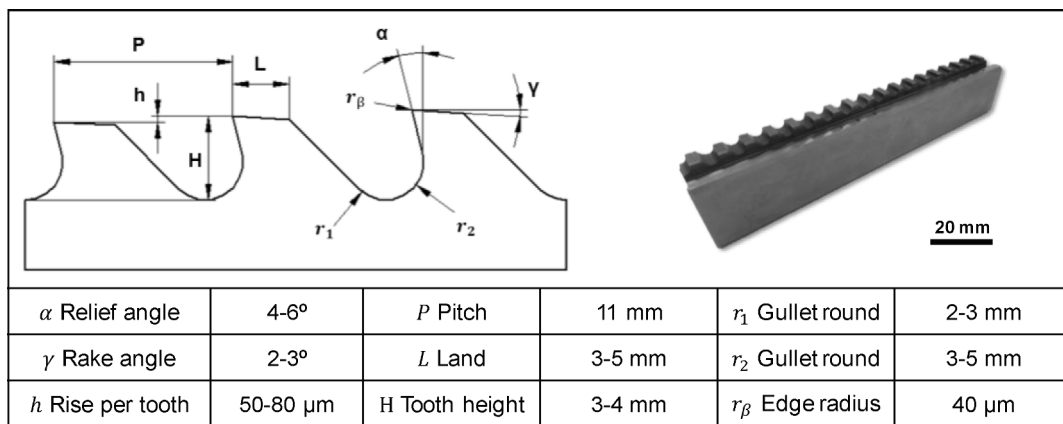
Material	Inconel®718
D	500 mm
d	370 mm
e	34 mm

Fig. 5. Test piece dimensions.

α Relief angle	4-6º	P Pitch	11 mm	r_1 Gullet round	2-3 mm
γ Rake angle	2-3º	L Land	3-5 mm	r_2 Gullet round	3-5 mm
h Rise per tooth	50-80 µm	H Tooth height	3-4 mm	r_β Edge radius	40 µm

Fig. 6. Geometry and general characteristics of the coated broaching tool (Tool A and B).

alloy presents a good behavior under extreme working conditions, even at temperatures above 873 K, and it keeps the mechanical properties: good resistance to fatigue, creep, and corrosion [23,24]. On the other hand, many manufacturing challenges appear, derived from IN718 elevated cutting force (specific cutting force is about 2800–3200 N/mm^2). A typical problem regarding tool health is the appearance of building-up edges and/or extreme tool edge chipping wear. Table 2 shows Inconel 718 composition and mechanical properties.

The test piece was a disk, similar but smaller than aeroengine turbine disks, Ø500 mm in external diameter and Ø370 mm in internal one, while thickness was 34 mm. The outer ring holes that can be seen in Fig. 5, guaranteed the stiffness of the part bolted onto the machine table. In addition, a little wider reference slot must be done to enable the part to return to the initial position on the bottom of the Z-axis, because broaching only works in one direction (ascending movement, up-stroke).

The testing broaching tool comprised three tool segments, for the initial roughing of fir-tree slots. In roughing, the slot shape was rectangular. Tools for roughing process are made of cemented carbide or other hard metals, while for finishing, tools in High-Speed Steel (HSS) are the main option, due to homologation procedures and standards in aircraft components manufacturing. Therefore, to test at higher cutting speeds, sintered carbide (type S10, grain 0,8-µm grain size, 10% Co) tools were used. Compared to high-speed steel, cemented carbide has significantly higher hardness and heat resistance, which allows increasing cutting speed, but it is very sensitive to vibrations so it tends to suffer cutting edge breakages, chipping, during machining. In this work, two different types of sintered carbide tools were tested: two tool segments with a coating (type AlTiN) and a last one without coating.

The cutting speed (V_c) is the only parameter that can be changed after a broaching tool is manufactured. Here, it was established at 19 m/min to work with straight cutting oil as coolant. Besides, turbine disk fir-tree slots were inclined 15°, typical in many turbine disks. So that inclination makes the tool engagement into the material to be gradual, but during the broaching process, cutting is completely orthogonal, since cutting speed is always perpendicular to the cutting edge. It should be pointed out that cutting conditions were chosen to values where no machine vibration due to natural frequency was found. Relevant information about the coated tool geometry is shown in Fig. 6. Here, *Rise per tooth* could be considered equivalent to feed per tooth in other machining processes. Milling depth and width of cut would be defined by other tooth differences, width change only a little.
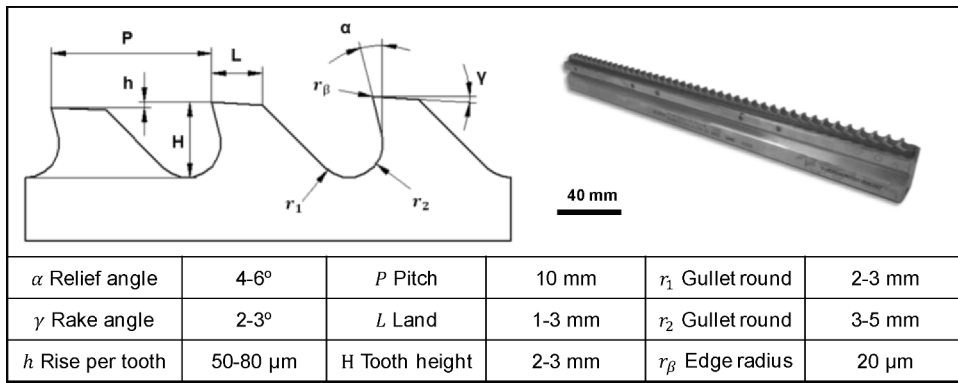
α Relief angle	4-6°	P Pitch	10 mm	r_1 Gullet round	2-3 mm
γ Rake angle	2-3°	L Land	1-3 mm	r_2 Gullet round	3-5 mm
h Rise per tooth	50-80 µm	H Tooth height	2-3 mm	r_β Edge radius	20 µm

Fig. 7. Geometry and general characteristics of the uncoated broaching tool (Tool C).
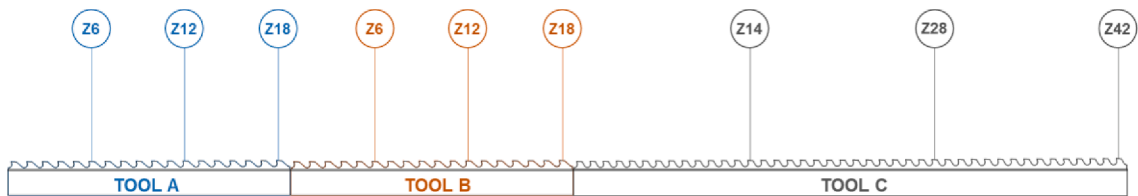
Fig. 8. Broaching tool assembly and cutting tool. Numbers are for controlled teeth. Cutting starts at the left.

In Fig. 7, general characteristics of the uncoated broaching tool are presented. The two coated tools were the same, with the same number of teeth, 18 edges. On the other hand, the uncoated tool had 42 edges, so altogether there were 78 cutting edges to analyze.

Fig. 8 shows the total assembly of the segments that complete the testing broaching tool, in a row. For convenience, each segment will be considered and named as a cutting tool (A, B, C) and 3 teeth (or cutting edges) will be analyzed on each segment to check the tool condition.

It was decided to use broaching tools with different characteristics to analyze how the signals collected by the devices change. Therefore, for these experimental trials we had 3 tools with two different typologies:

- Type 1: Tool A and Tool B (Coated cemented carbide tools)
- Type 2: Tool C (Uncoated cemented carbide tool)

Another difference between tools, besides the coating, was the distance between consecutive teeth. From a monitoring point of view, this means that the frequency at which teeth penetrate into the workpiece, named "tooth passing frequency" or "striking" one, was different. This factor was very important when choosing the correct bandwidth of the measurements devices to prevent from losing any kind of information.

$$T_{pf1} = \frac{V_c}{P_1} = \frac{15-20m/min}{10-12mm} = 20.83 - 33.33Hz(ToolA) \tag{1}$$

$$T_{pf2} = \frac{V_c}{P_2} = \frac{15-20m/min}{10-12mm} = 20.83 - 33.33Hz(ToolB) \tag{2}$$

$$T_{pf3} = \frac{V_c}{P_3} = \frac{15-20m/min}{9-11mm} = 22.72 - 37.03Hz(ToolC) \tag{3}$$

For all measuring devices, sampling frequency was at least twice the "tooth passing frequency". Another relevant difference between the two types of cutting tools was the number of teeth engaging into the workpiece at the same time. According to [25-27], the number of effective teeth at the same time increases broaching force proportionally, as may be seen in Eq. (4).

$$F_C = b \times h \times K_s \times Z_e \tag{4}$$

It was essential to estimate the broaching cutting force to avoid overpassing any machine safety limit. For the calculation of effective teeth (Z_e) the thickness of the work-piece (e), the broach pitch (P) and the land of the tooth (L) must be taken into account. The value of the effective teeth amount is calculated in Eqs. (5), (6), (7).
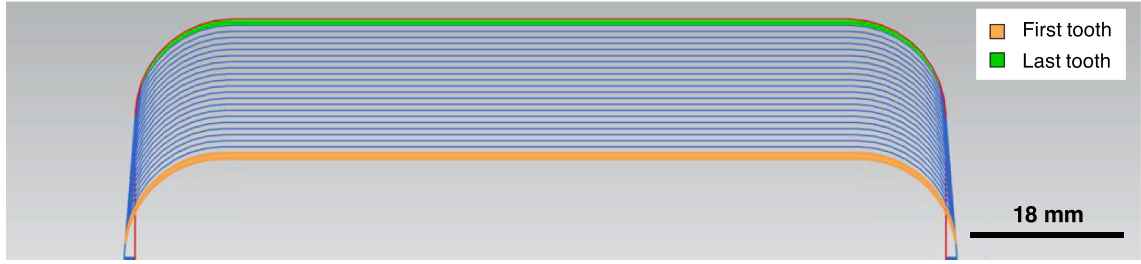
Fig. 9. Evolution of the teeth dimension along tool length: rise per tooth and light width of cut. Section shape is slightly trapezoidal.
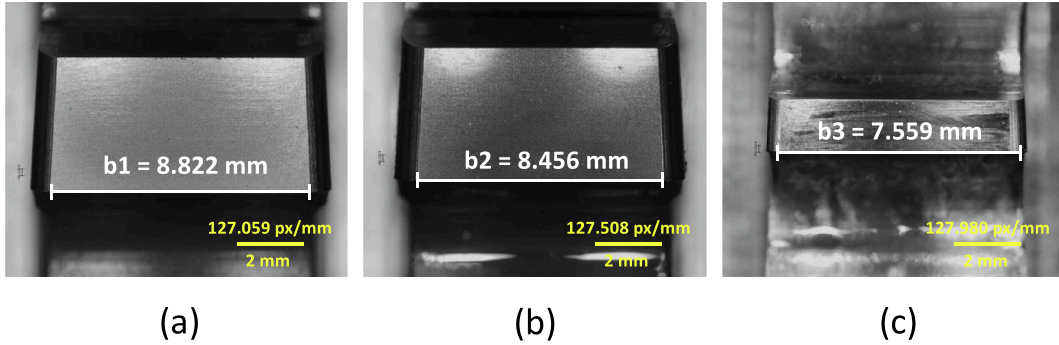

Fig. 10. **(a)** Tool A, mean width **(b)** Tool B, mean width **(c)** Tool C, mean width.

$$Z_{e1} = \frac{e}{P_1 \times cos15^o} = \frac{34mm/cos15^o}{10-12mm} = 2.93 - 3.52 \approx 4 teeth (ToolA) \tag{5}$$

$$Z_{e2} = \frac{e}{P_2 \times cos15^o} = \frac{34mm/cos15^o}{10-12mm} = 2.93 - 3.52 \approx 4 teeth (ToolB) \tag{6}$$

$$Z_{e3} = \frac{e}{P_3 \times cos15^o} = \frac{34mm/cos15^o}{9-10mm} = 3.20 - 3.91 \approx 4 teeth (ToolC) \tag{7}$$

Some three teeth are always cut and sometimes four. The tooth width (b) and Rise per tooth (h) were known values, but it had to be taken into account that the tooth width varies slightly along with the broaching tool, as is shown in Fig. 9.

For that reason, for average cutting force theoretical calculation, a mean value was used, which corresponds to the middle tooth width value of each broaching tool. This measurement is shown in Fig. 10.

On the other hand, specific cutting force parameter (K_S) values depend on work-piece material, which for IN718 typical values are between 3000 and 3200 N/mm^2. So, the cutting force for each tool would be approximately Eqs. (8)–(10):

$$\boldsymbol{F_{C1}} = \boldsymbol{b_1} \times \boldsymbol{h_1} \times \boldsymbol{K_s} \times \boldsymbol{Z_{e1}} = 5,800 - 8,500N \tag{8}$$

$$\boldsymbol{F_{C2}} = \boldsymbol{b_2} \times \boldsymbol{h_2} \times \boldsymbol{K_s} \times \boldsymbol{Z_{e1}} = 5,400 - 7,600N \tag{9}$$

$$\boldsymbol{F_{C3}} = \boldsymbol{b_3} \times \boldsymbol{h_3} \times \boldsymbol{K_s} \times \boldsymbol{Z_{e2}} = 5,000 - 7,200N \tag{10}$$

This calculation ensures that the maximum cutting force allowed by the machine was not exceeded, which for the Ekin® A218/ RASHEM broaching machine is 70,000 N, so real values would be far from the maximum one.

2.3. Sensors location

It was of utmost importance in order to minimize signals attenuation, to mount sensors close to the cutting zone. In this case, it was impossible to place the sensors exactly in the cutting area. Therefore, it was decided to place the load cells on the back support between the workpiece disk and the rotary indexing table. In Fig. 11 the two load cell positions are shown. Two load cells were placed to balance the measurement during the machining process.

Regarding accelerometers, a similar problem was faced up. Since the broaching machine system have two different parts: a mobile (onto which piece is located) and a static one (where the tool is fitted), two different sets of accelerometers had to be placed to record
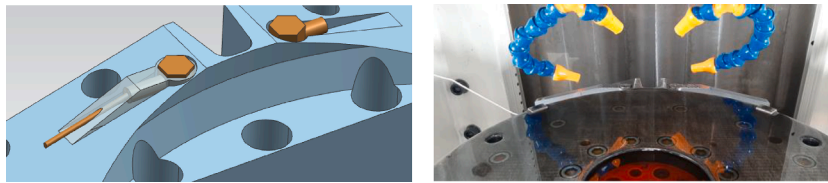
Fig. 11. Load cell location during monitoring, at both sides of the machined slot.
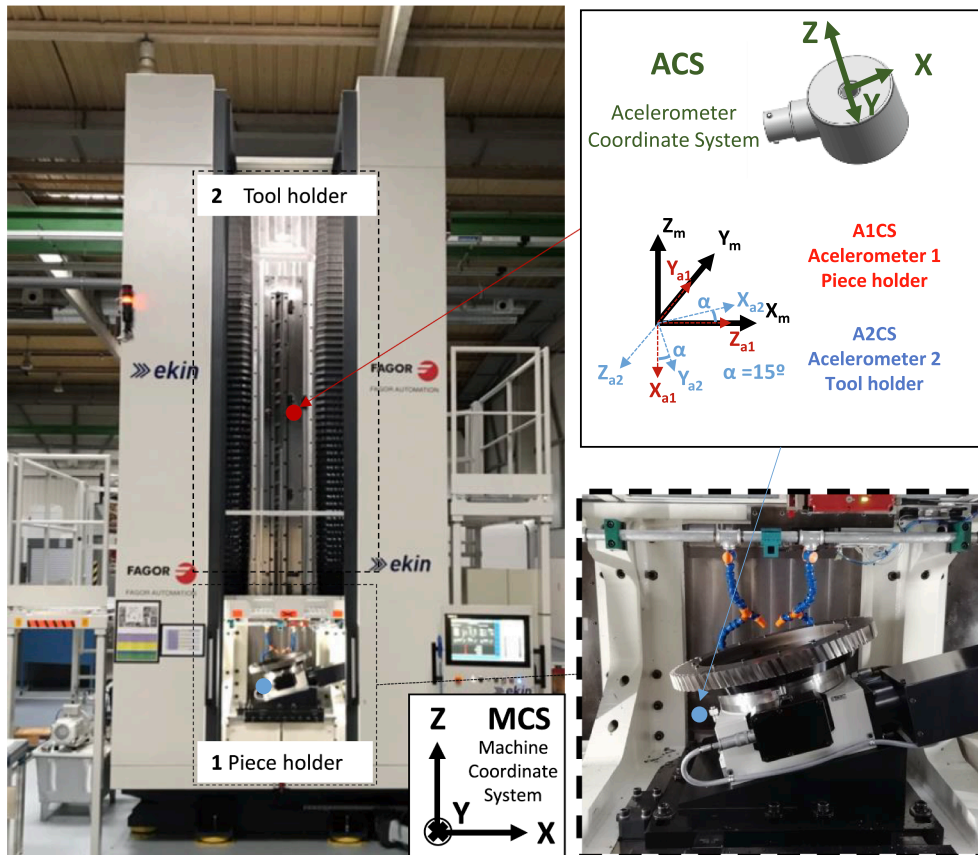

Fig. 12. Schematic diagram of the monitoring system: points mark accelerometers in the moving table or in the machine column.

process vibration. Besides, the position of the devices had to avoid the nodes of the column main nodes. Each accelerometer had de capacity to measure the accelerations in 3 directions, defining a local coordinate system. Since the indexing rotary plate was turned 15° in Y-axis, at least 2 directions of the accelerometer do not coincide with the machine global coordinate system. Accelerometer locations are shown in Fig. 12. In order to simplify measurements understanding, all accelerometer signals results were named based on the machine global coordinate system.

3. Results

In this section, each process output variable is explained. In addition, a correlation between signals and tooth flank wear value is discussed.

3.1. Tool wear

In the verification testing campaign, the three-tool segment tools machined a total number of 90 full slots, using straight oil (CUT-MAX S 50259-1) coolant. Tool wear occurs mainly on edge flank surfaces (so-called flank wear VB), but it can also appear on the rake face as crater wear. Wear causes can be multiple and occur simultaneously. However, the most common one is abrasion. Some amount
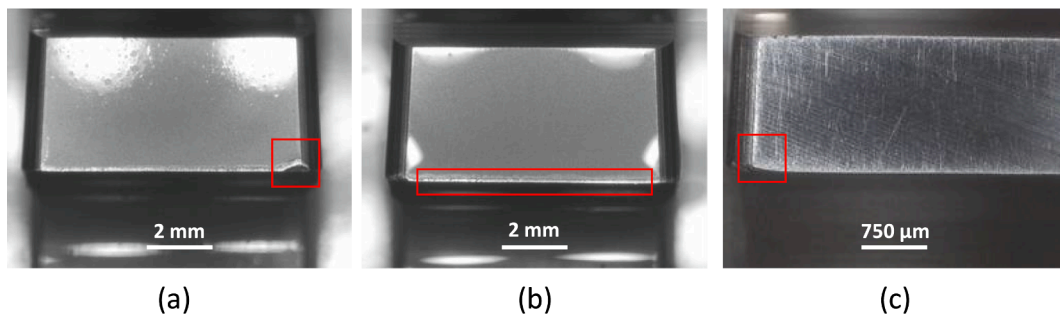
Fig. 13. Types of wear found during the experimental testing **(a)** Tooth fracture **(b)** Flank tool wear, more common **(c)** Plastic deformation of the tip.
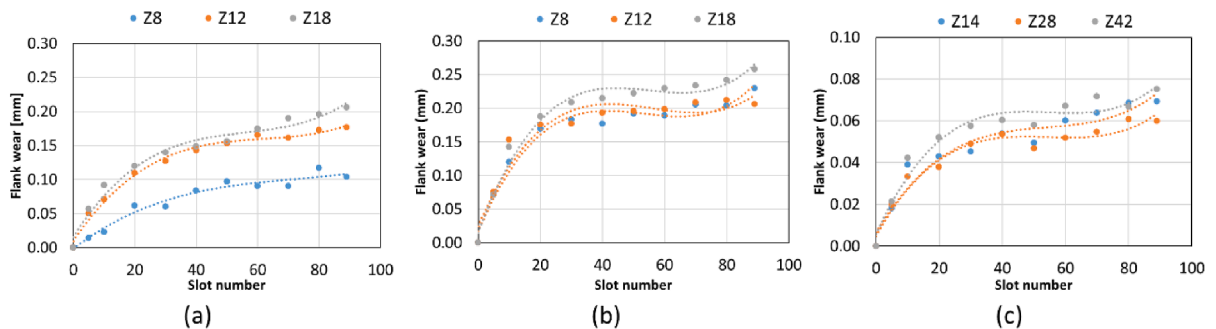
Fig. 14. Flank tool wear evolution during broaching, a) Tool A, b) Tool B and c) Tool C.
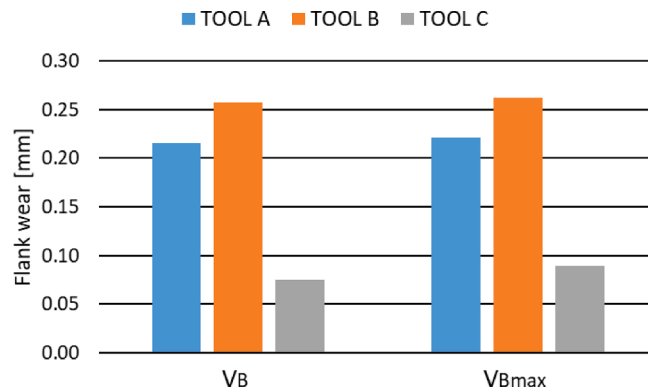
Fig. 15. Tool wear for each tool last cutting edge after machining 92 slots.

of plastic deformation can also appear at teeth tips. Edge chipping due to unexpected vibrations can also happen. Other mechanisms more temperature-dependent are not common, because process temperature is kept by coolant oils.

Fig. 13 illustrates different kinds of tool wear recorded during INCONEL® 718 broaching process. Type b) is the usual measured and included in graphs.

Regarding results, the coated tools showed higher wear than the uncoated tool. Regarding tooth function, it is the third tooth of the first segment (Tool A) considered the starting one, while the first and the second teeth are only a security distance left to avoid a fatal collision at the tooth entrance. Tool A showed several tooth breaks in the corner, which appeared specifically on cutting edges number 5, 6, 7 on the right corner of the broach. Due to the 15° inclination (counter-clockwise), the right corner is where the tool starts engaging the workpiece, with some hits against the disk ring. Besides, all cutting teeth suffered flank wear not very uniform. Because many teeth were chipped, flank wear values increased in nearby zones. Tool B, on the other hand, did not show any tooth break and showed progressively uniformly flank wear along the cutting edge, which is interesting for achieving a stable process. Finally, Tool C, which corresponds to the uncoated tool, also showed flank wear, but lower than the coated tools, with the peculiarity that in some teeth the corners were more worn out due to possible plastic deformations. As Tool A, Tool C presented one chipped tooth, the last one.
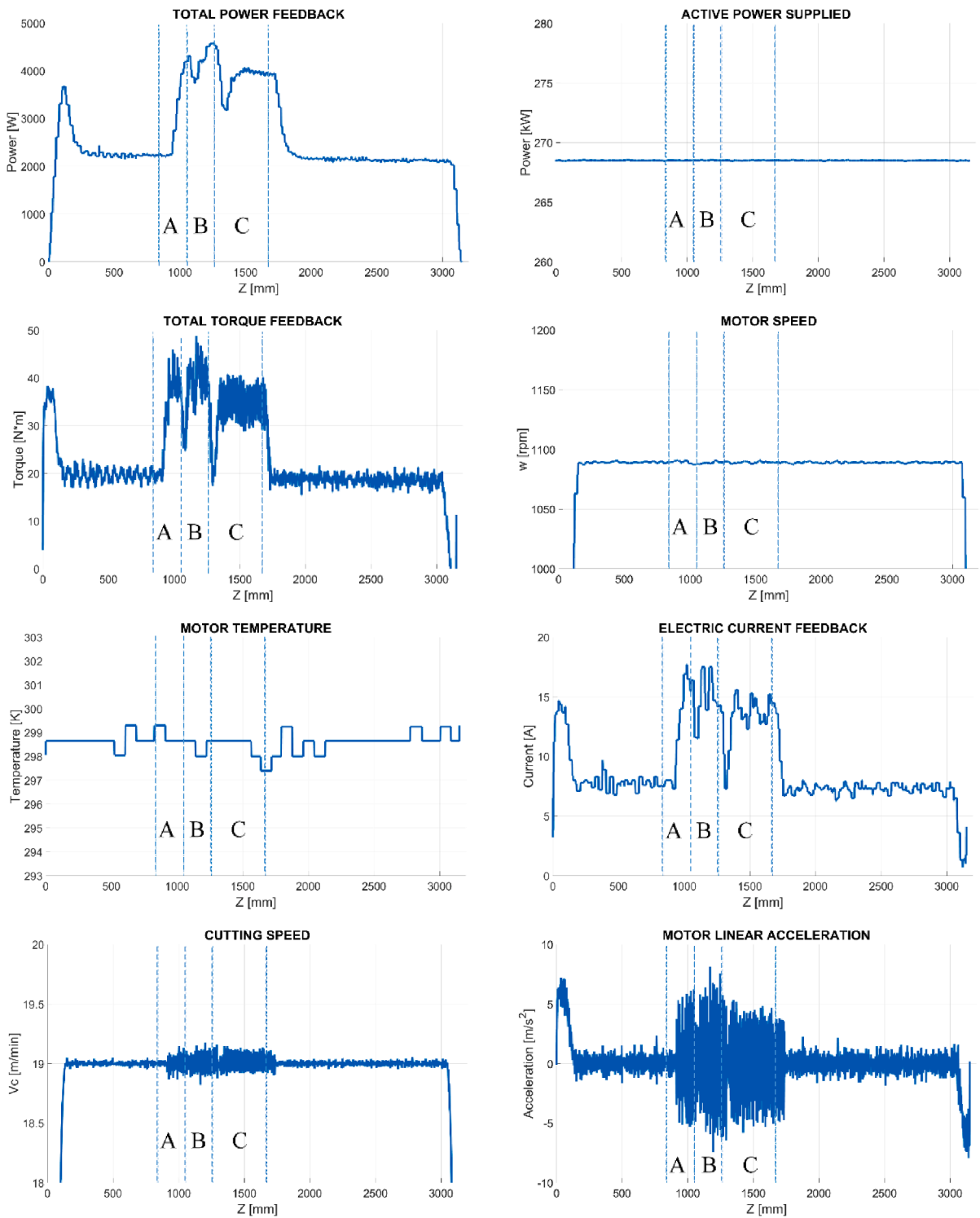
Fig. 16. Information collected from motor drivers, taking from machine PLC, recording zones for Tools A,B,C are shown. Peaks at time zero is because initial acceleration without cutting.

Even so, flank tool wear evolution for the 3 tested cutting tools was deeply analyzed to gain knowledge about each tool performance. It was decided to evaluate 3 different sections of the tools to have an average value of the real tool wear. These 3 sections were: the entry of the tool (engaging zone) into the material, the stable cutting zone (middle zone), and the tool exit (final zone). So, for Tool

Table 3

Mean values of recorded machine data along the broached length (calculated as 92 slots × disk thickness).
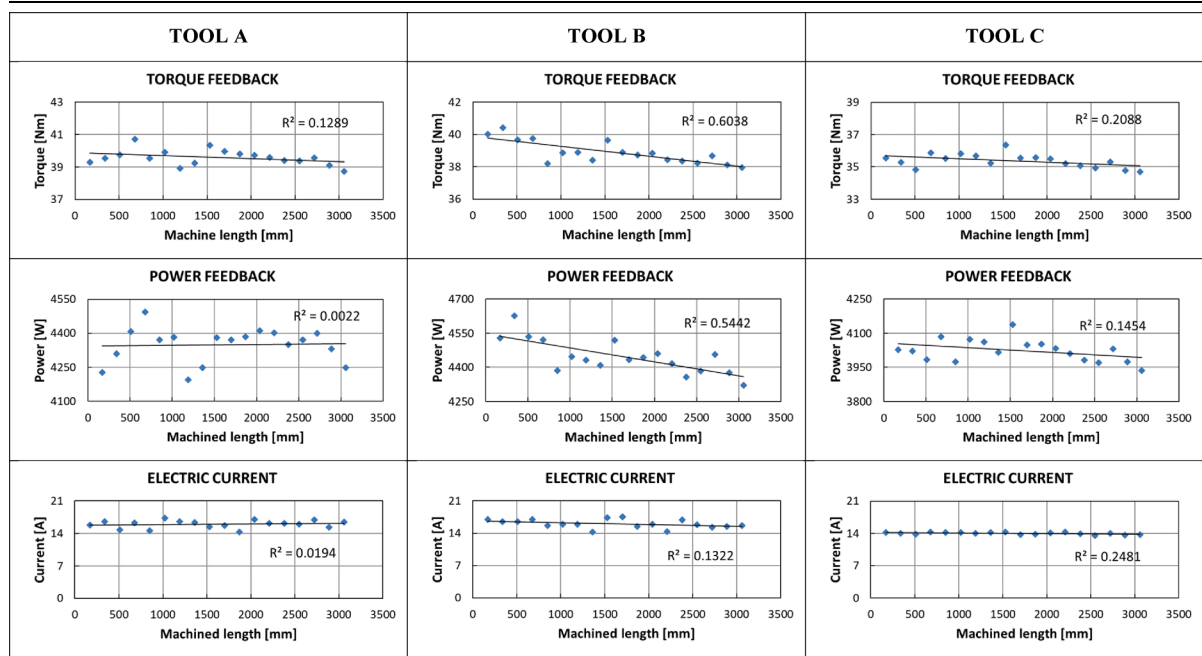
A and Tool B teeth 6, 12, and 18 were examined, while for Tool C teeth 14, 28, and 42 were examined.

The evolution of cutting-edge wear is illustrated in Fig. 14. Firstly, it was observed that wear results were similar to a typical 3-stages wear pattern evolution (childhood, maturity, old age): The initial rapid wear zone (slot 5 to slot 40), a uniform wear zone (slot 40 to 80), and in some cases the acceleration wear zone (slot 85 onwards), corresponding to a region of final failure.

As visualized in Fig. 15, the last 3 edges of each broach showed the highest wear, the reason is the trend of Inconel to *strain hardening*, each tooth deforms and hardens the machined surface, so the last operation suffered the cumulative strain hardening effect. It can be noticed that given the same broaching conditions, Tool B – Z18 suffered higher wear than Tool A – Z18, almost 25% more and 3.4 times more than Tool C – Z42.

3.2. Motor driver signal processing

A common practice to determine tool wear is by collecting cutting force. However, this method may not be technically suitable for the industry. On the other hand, internal signals and machine-tool data are presented as a possible solution to quantify tool wear. As previously mentioned, the motor drivers lecture was acquired using a Fagor® software program through PLC system. In Fig. 16 all recorded data from motor-driver is presented.

Signals would be motors active power feedback, rotatory speed, motor temperature, and cutting speed, in the figure the three segments are shown. The latter did not display the difference between the three tool segments. For the former ones, it can be seen that signals are divided into an idle time and a machining one. Thus, broaching machining time is divided into three that correspond to each segment (A,B,C). After classifying which signals provide sensitive information, an analysis was performed in order to relate how signal values vary according to tool wear. To do so, the following analyses were performed:

- In the time domain, a comparison using the mean and maximum values of power, torque, and electrical current was performed (using the sum of both servo-motors).
- Motor linear acceleration values were also transformed to the frequency domain through a fast Fourier transform (FFT) algorithm. The frequency range was half of the bandwidth (250 Hz): 0–125 Hz (so, this included the tooth passing frequency).

In Table 3 the evolution of servomotors power, torque and electric current consumption average values along 90 full slots produced is shown. Thus, the first row shows the sum of the torque generated by the motors to move the part. This value not only changes between different tools but also over the lifetime of the tools. At a first glance, for all tools, torque value has a decreasing trend. However, it is only Tool B that shows a high correlation with tool wear $R^2 = 0.608$, while Tool A and Tool C show a noticeably smaller correlation, $R^2 = 0.128$ and $R^2 = 0.208$.

Table 3 next row displays the sum of power consumption of both servomotors. As with torque, power values vary for each tool position and tool type, as well as, by suffered flank wear. This time, the three tools show different trends, but once again, it was Tool B

Table 4

Maximum values of recorded machine data along the broached length (92 slots × disk thickness).
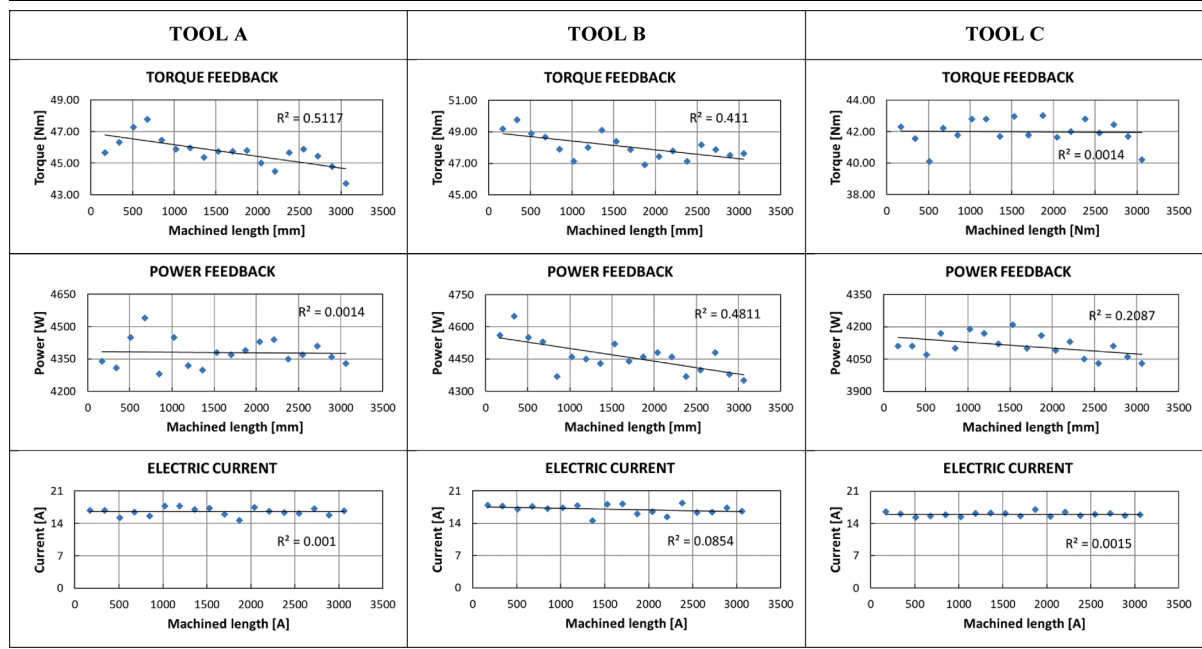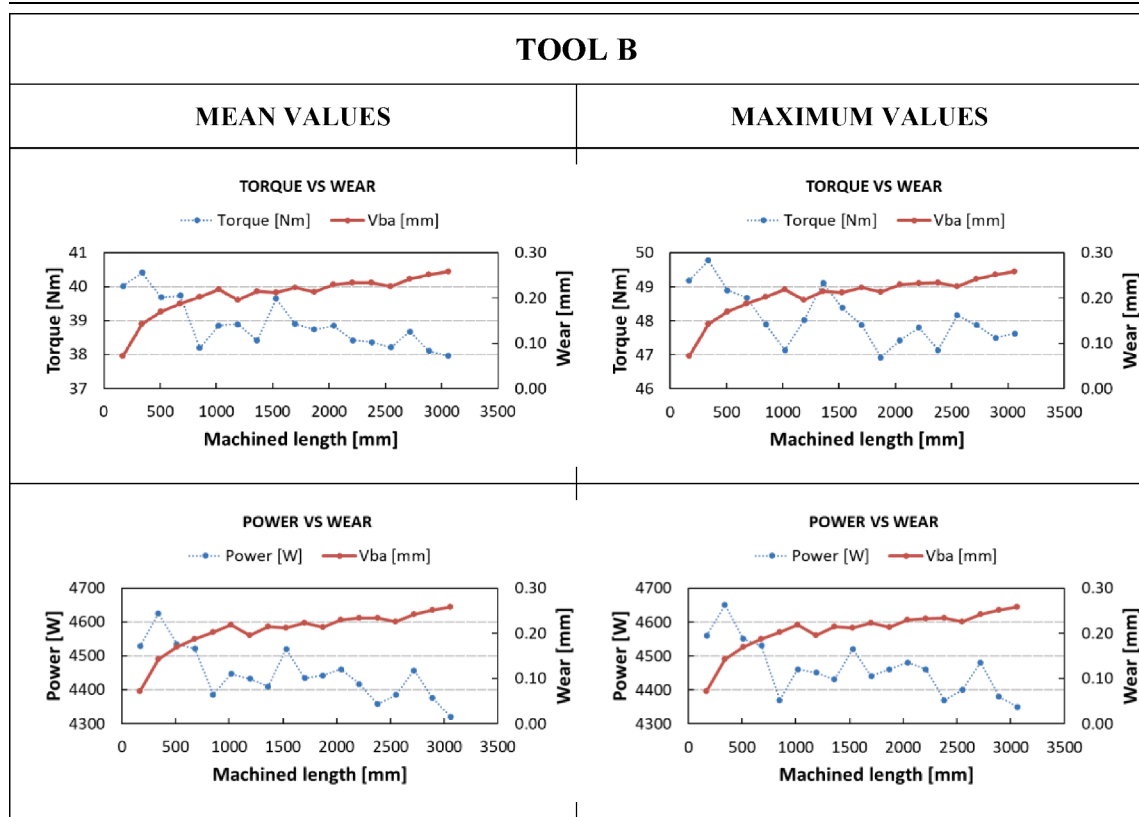

Table 5

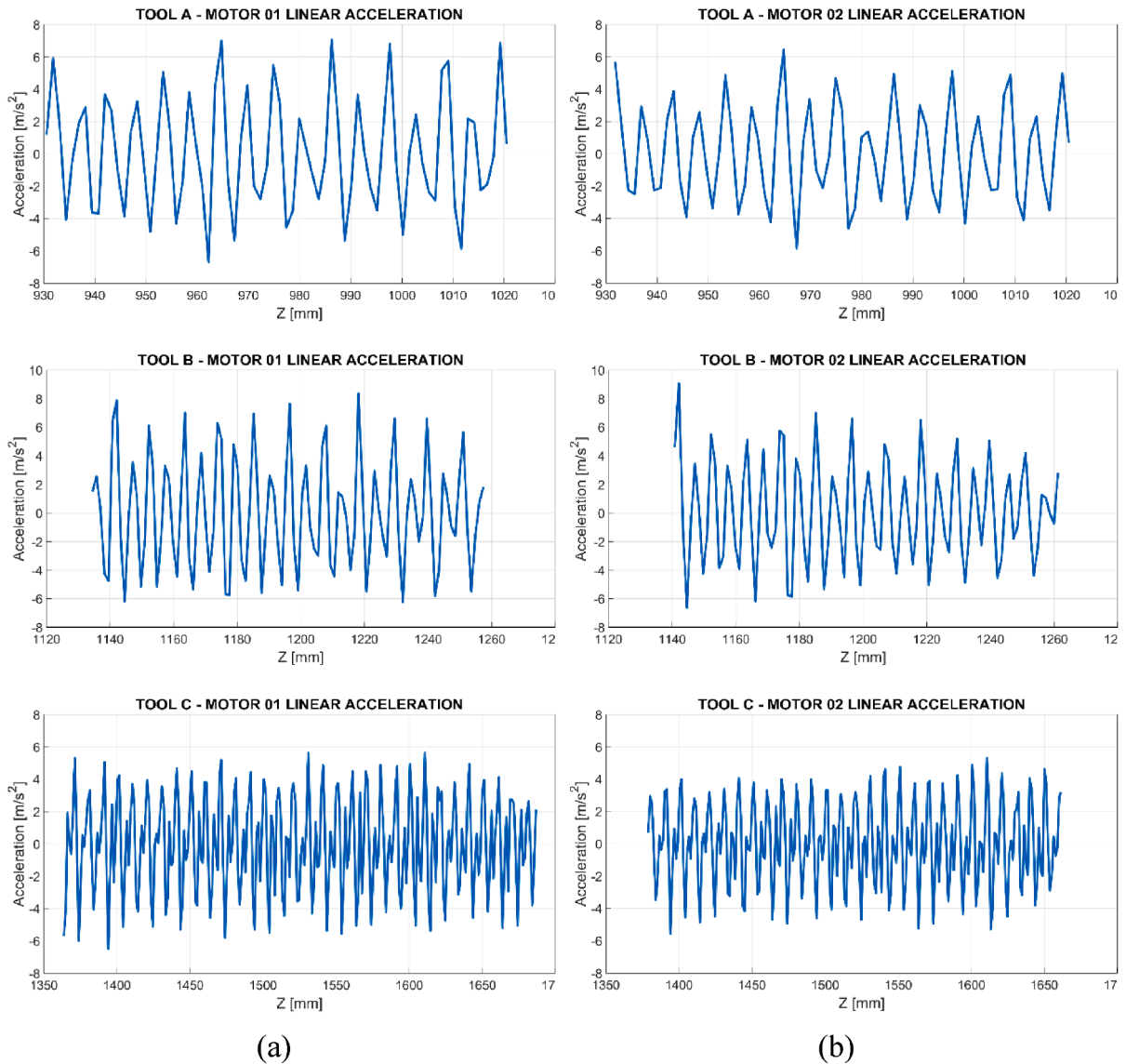Visual relation between relevant motor signals and Tool B flank wear.

Fig. 17. (a) Motor 01 linear acceleration divided for each cutting tool **(b)** Motor 02 linear acceleration divided for each cutting tool.

that showed to have the bigger influence by edge wear $R^2 = 0.544$, followed by Tool C with a $R^2 = 0.145$. On the contrary, power consumption while Tool A is working remained steady with a correlation value of $R^2 = 0.002$. The final row presented the sum of the electrical current employed by two motors during the broaching process. As far as can be observed, this value does not seem to have a great influence in describing the Tool Condition, since for all the three tools the values of the electric current of the motors are stable. The correlations parameters are for Tool A, $R^2 = 0.019$, Tool B, $R^2 = 0.132$ and Tool C, $R^2 = 0.248$.

In Table 4 a similar analysis to the one carried out for the mean values is performed, but on this occasion with maximum values of servomotors power, torque, and electric current consumption along with the all broaching tests. Maximum values vary according to the Tool And cutting edge wear range. For the torque feedback case, Tool A shows the highest linear correlation, $R^2 = 0.511$, followed by Tool B $R^2 = 0.411$ (Table 5).

Nonetheless, Tool C does not present any correlation with flank wear $R^2 = 0.001$. When it comes to power feedback, Tool B exhibit the greatest linear correlation $R^2 = 0.481$ and then Tool C $R^2 = 0.1454$. Tool A, once again, does not show any correlation with flank wear, $R^2 = 0.001$. Similarly to mean values, maximum values of electrical current did not give any information about tool wear condition, where the linear correlation parameters are for Tool A is $R^2 = 0.001$, Tool B is $R^2 = 0.085$, and Tool C is $R^2 = 0.001$.

All in all, servomotor power and torque values provide valuable information about cutting process performance. On the contrary, motors electrical current does not shed any light on the tool condition and is therefore not a relevant parameter to monitor. On the other hand, it seems that these two motor signals do not seem to be able to represent the broaching process when the broaching process has not yet stabilized. For this reason, the wear of Tool A cannot be well represented only with the signals obtained. At the same time,
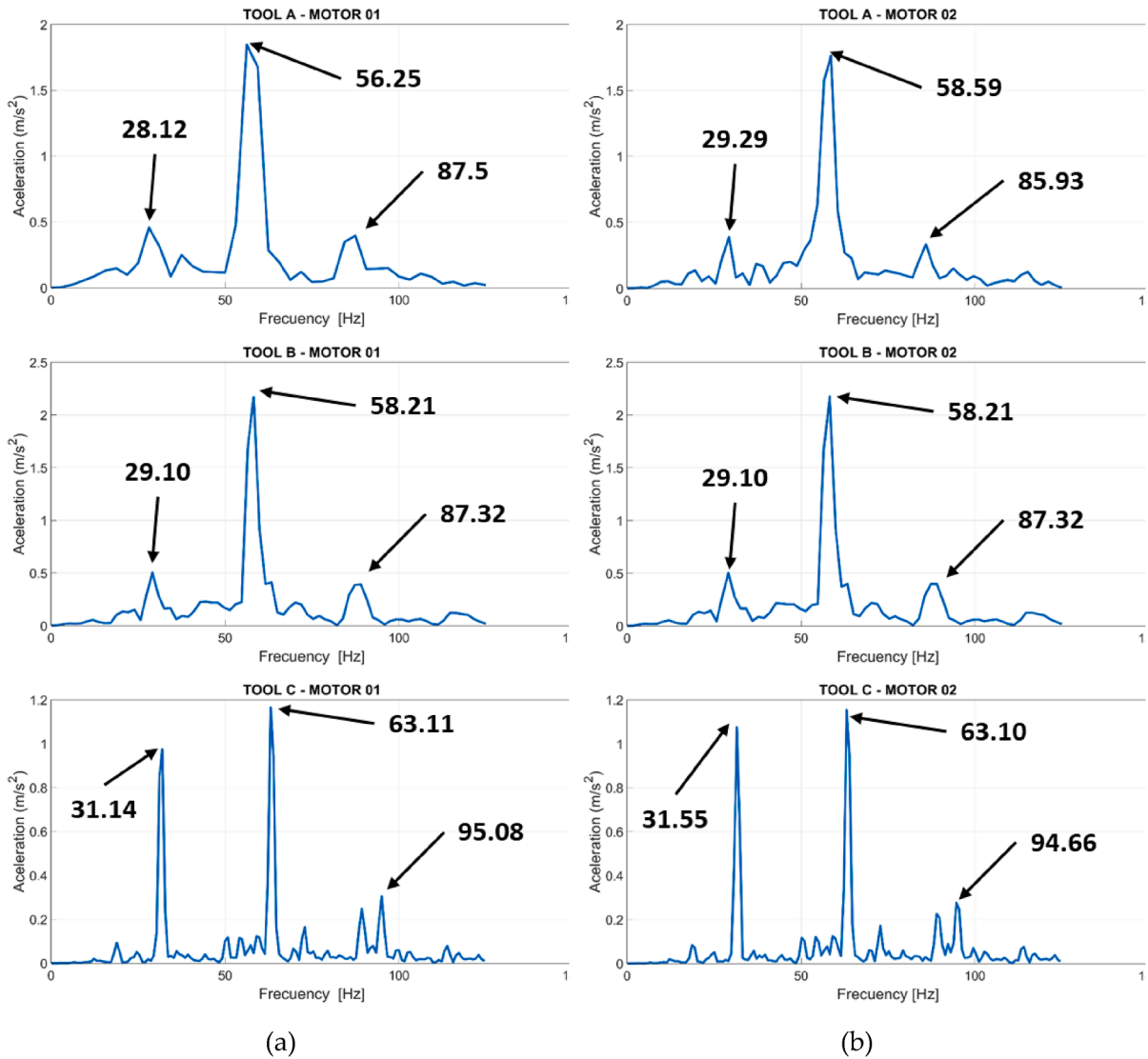
Fig. 18. (a) Linear acceleration of the motor 01 in the frequency domain **(b)** Linear acceleration of the motor 02 in the frequency domain.

Tool C cannot be also well represented since his flank wear value is too small, around 0.07 mm. Tool B is the only one that was monitored since the cutting process is stable and the tool wear is notorious, around 0.2 mm.

In order to analyze the existence of any relation between motors acceleration and flank tool wear, more work was needed. Since time-domain does not offer much information, it was better to evaluate the signals in the domain of frequency, and so look here for any trend. In Fig. 17 the motor accelerations are presented during each tool working range in the up-stroke vertical movement.

Once all the acceleration signals were recorded, the analysis started by applying a Hanning window filter to apply the Fast Fourier Transformation (FFT) and obtain the harmonic frequencies during each pass of the broaching cycle. On this occasion, there was no need to apply any low pass filter, after all, the acceleration signals from two motors were acquired at a very low frequency, with a band frequency of 125 Hz and therefore a sampling frequency of 250 Hz. In Fig. 18 each motor acceleration is converted in the frequency domain

So, both servomotors have two main harmonic frequencies for each broaching tool, which are regular multiples of the tooth passing frequency for each tool. The amplitude of each harmonic frequency could not be an absolute value, but they may be linearly related to the actual motor linear acceleration. By monitoring these amplitudes as cutting tools suffer from wear, it is possible to find a correlation for tool performance monitoring. Thus, in Table 6, Table 7, and Table 8 the evolution of harmonic frequency amplitudes of *servomotor 01*, *servomotor 02*, and the sum of both during broaching tests are presented. Table 6 displays the motor linear acceleration evolution while Tool A is working. As Tool A is the first tool to enter the workpiece, the material cut is not stabilized, so the values of the frequency amplitudes do not provide any relevant information. The best linear correlation parameter obtained was for motor 02, tooth passing frequency $R^2 = 0.517$. Table 7 exposed the same information, but for the cutting Tool B. When Tool B is working, the process

Table 6
Tool A harmonic frequency amplitude evolution during broaching process.
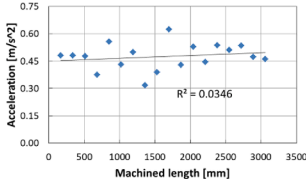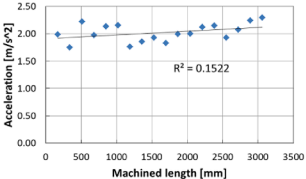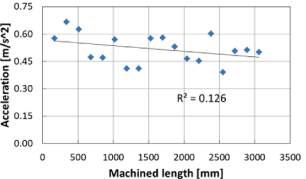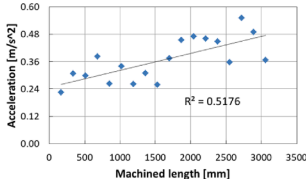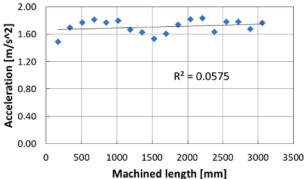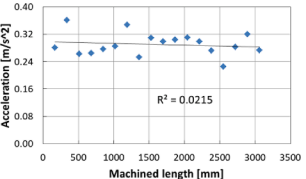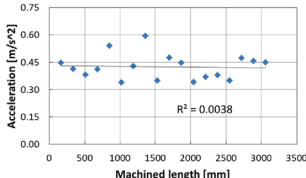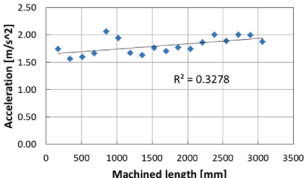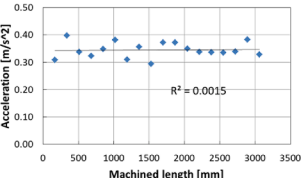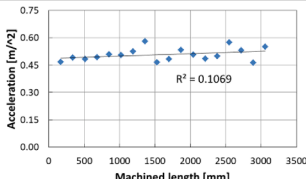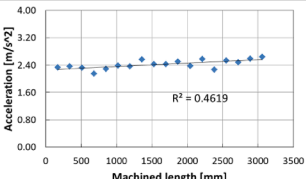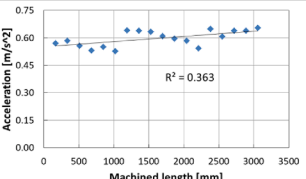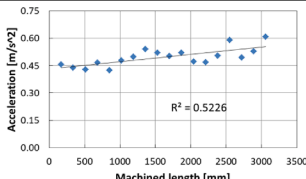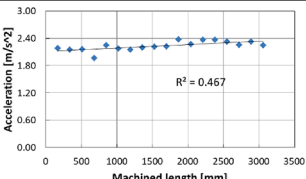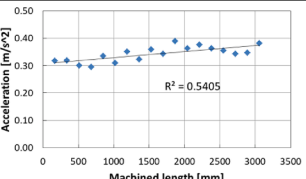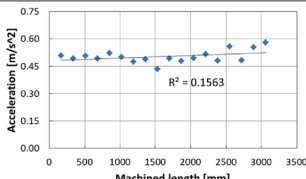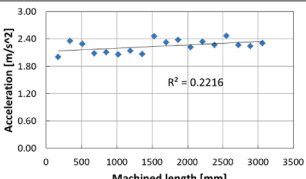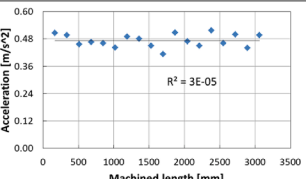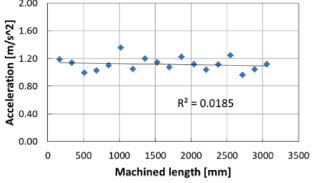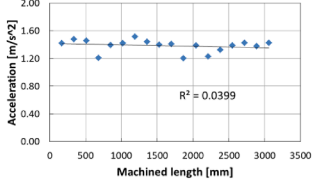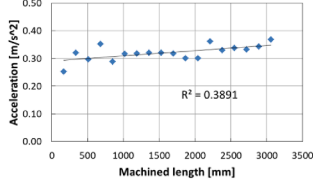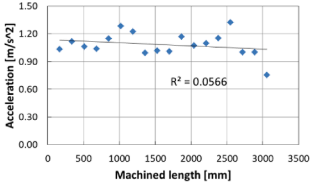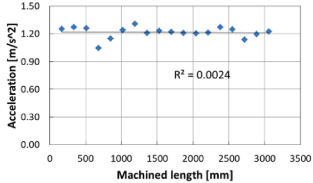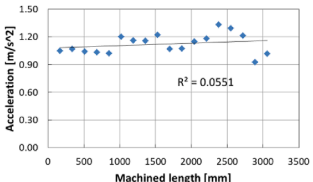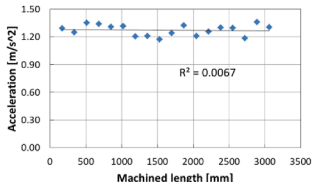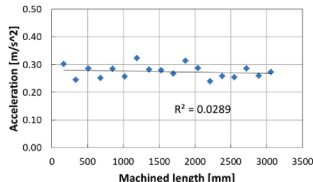

Table 7
Tool B harmonic frequency amplitude evolution during broaching process.

can be said to become stable, so that signal values obtained are more significant.

This is shown by the values in Table 7, where almost all of the natural frequencies amplitudes show a certain relationship with tool wear, especially the signal from servomotor 02. This may be due to the gantry system that moves the workpiece to produce the machining. Although the two motors are synchronized, one motor works harder on the upstroke (broaching) and the other on the descent (no working). The best linear correlation parameter obtained was with motor 02, second harmonic frequency of tooth passing

Table 8
Tool C harmonic frequency amplitude evolution during broaching process.
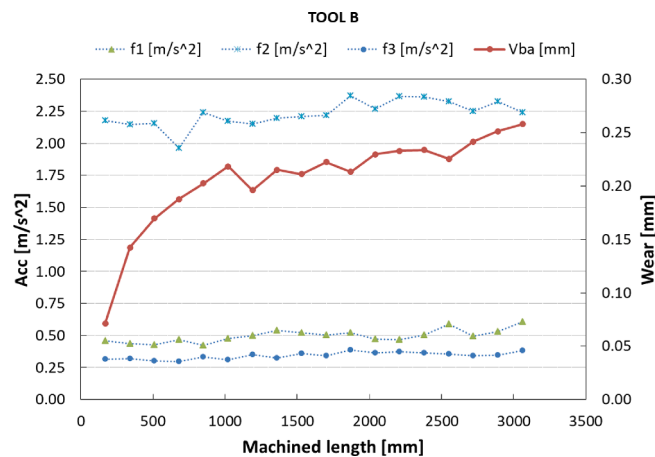
Fig. 19. Tool B last cutting edge: flank wear evolution and relevant harmonic amplitude evolution of *servomotor 02*.

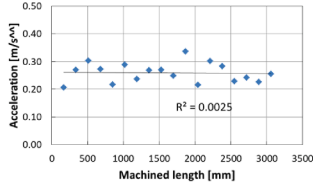frequency $R^2 = 0.540$. Finally, Tool C, which has the least wear at the end of the tests, has the lowest linear correlation of the three tools due to the fact that the cutting edges have not yet been worn out too much. This fact can be seen in Table 8, where the best correlation is obtained with motor 01, using the second harmonic frequency amplitude evolution, with an $R^2 = 0.389$.

In light of the result achieved, Tool B is the only one with some correlation with a) the signals acquired from the linear acceleration of the motors, especially motor 02 and b) flank wear, as it is shown in Fig. 19, where *f1* refers to tooth passing frequency and *f2* and *f3* to the two harmonic frequency. However, it should be noted that for this occasion the sampling frequency was limited to 250 Hz, so some process information may be missing. Therefore, it is necessary to contrast these data obtained with other equipment providing a higher sampling capacity, such as accelerometers, which directly measure the vibration in situ, without the noise generated by the machine electronics, and with a higher acquisition frequency.

3.3. Accelerometers signal processing

This section analyses the signals obtained with a measurement device with a higher sampling frequency, two ICP® triaxial

Fig. 20. **(a)** Broaching cycle accelerometer measurements in one slot, in Z-axis **(b)** Tool A broaching process acceleration divided in machine coordinate system (MCS).
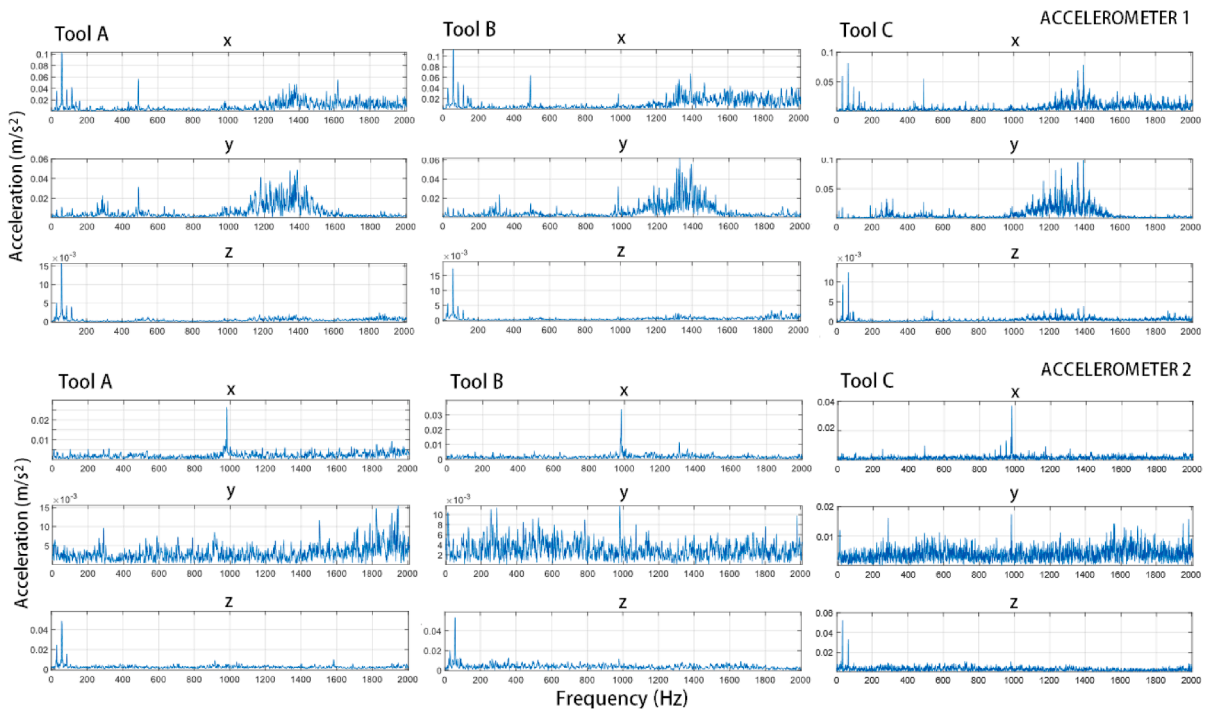
Fig. 21. Frequency spectrum of acceleration for each cutting tool corresponding to the machine coordinate system (MCS).

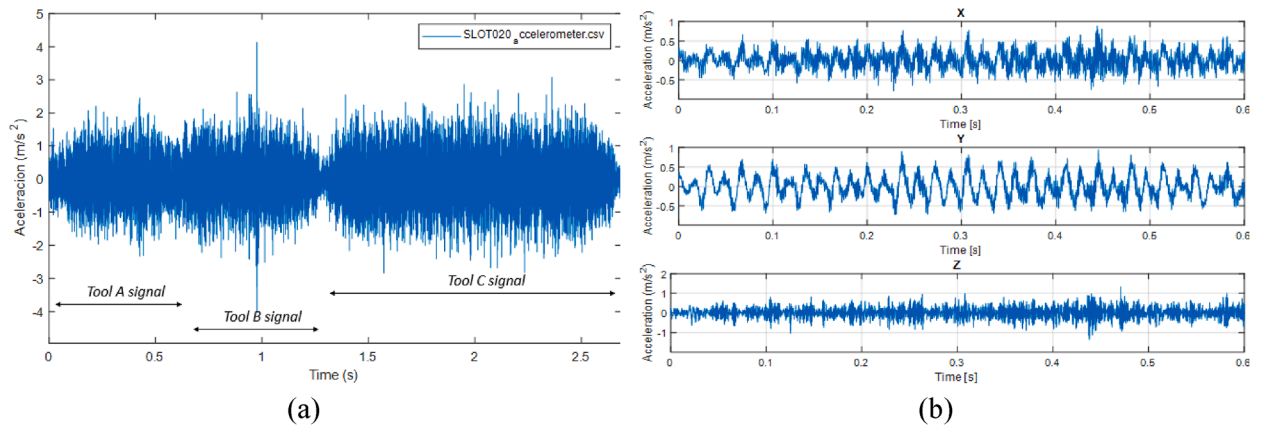accelerometers. Monitored signals are shown in Fig. 20. As the broaching process is considered an orthogonal machining process but workpiece is mounted inclined, it was convenient to obtain the signals based on the X, Y, and Z components. In broaching, the cutting direction is machine Z-axis, and the thrust direction is given by the normal of machined surface (machine Y-axis).

For a better study of the relationship between acceleration and wear, signals were analyzed in the frequency domain. Besides, a Hanning window was applied to use the Fast Fourier transform- Also some low-pass filters were used to find the position of high peak acceleration behavior in the spectrum. A normalized acceleration spectrum of acceleration versus frequency can provide useful information about tool condition. The spectrums were referenced to the machine axes of accelerometers 1 and 2 and they are shown in Fig. 21. The signals obtained from Slot 20 applying a low-pass filter of 2000 were taken as a reference, this was in the slot where a higher slope wear growth was denoted, as evidenced in Fig. 21. The vibrational spectra obtained from accelerometers 1 and 2 show different behavior. This is due to the stiffness at the points where the accelerometers influenced vibration values. Nevertheless, the behavior of the accelerations is similar between the 3 broaching tools in the X, Y, and Z components. The signal noise of accelerometer 1 is noticeable in the X component from frequency 1200 Hz onwards and in the Y component in the frequency threshold from 1000 to 1600 Hz. On the other hand, the noise is large in the Y component along the whole vibration spectrum, but its magnitude is smaller
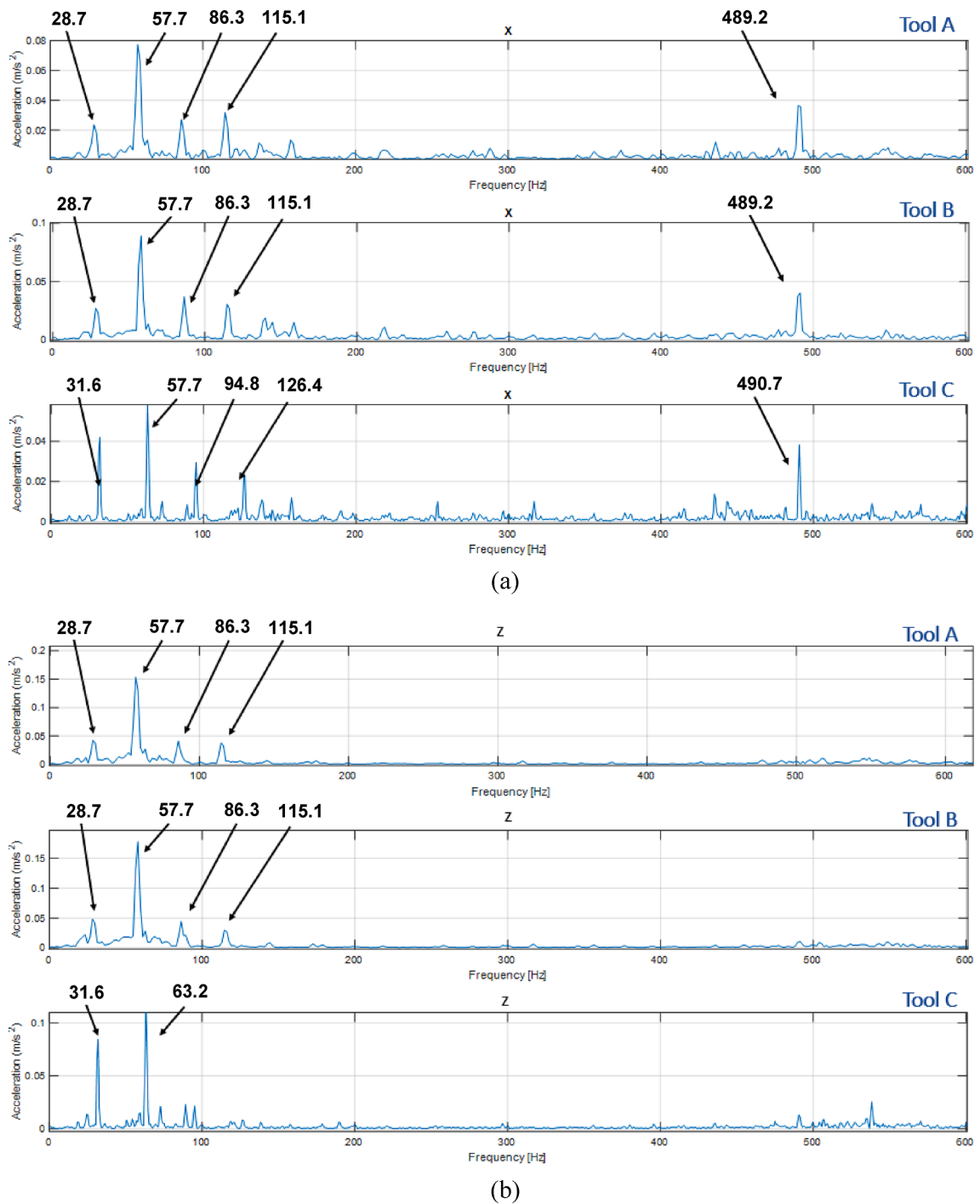
Fig. 22. Characteristic frequencies in the different broaching cutting tools for machine coordinate system (MCS): **(a)** X-component **(b)** Y-component.

than the noise presented in *accelerometer 1*.

Special attention was paid to vibration in the main and thrust cutting directions (Y-axis and Z-axis machine respectively) because it influences accuracy and surface quality. Therefore, from this point hereinafter, interpretations are based on these components. The main frequencies obtained from *accelerometer 1* are presented in Fig. 22, applying a low pass of 1000 Hz. For tools A and B, the characteristic frequencies of the broaching process were around 28, 57, 86, 115 and 490 Hz in the X component and 28, 57, 86 and 115 Hz in the Z component respectively. The signal in the Y component does not offer relevant information. On the other hand, for Tool C,
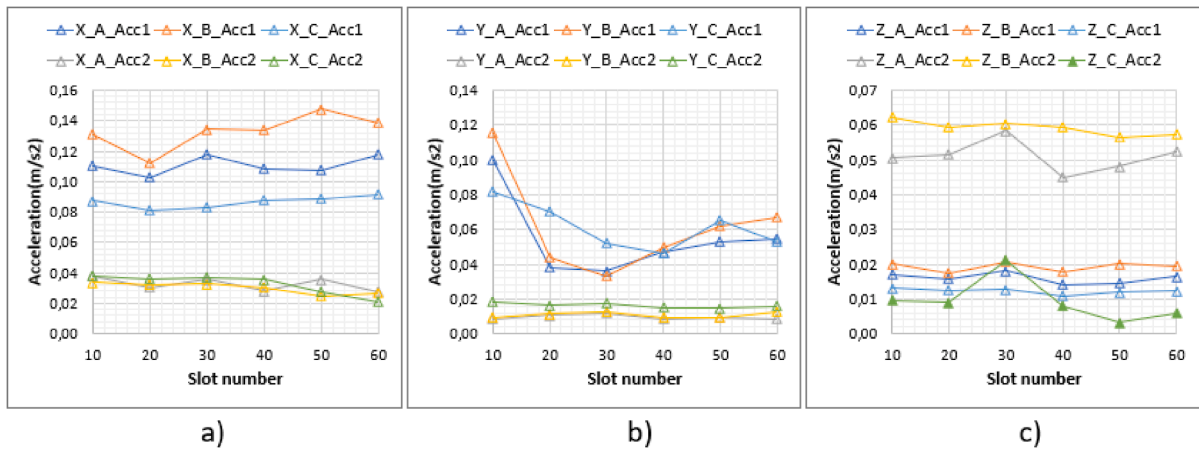
Fig. 23. Maximum amplitude accelerations of accelerometers 1 and 2 during each slot: **(a)** X component **(b)** Y component and **(c)** Z component.

Table 9
Provides the labels assigned to the data obtained from the accelerometers, Figs. 21-27.

				Broaching tool segments		
				Tool A	Tool B	Tool C
Accelerometers	01	Machine coordinate reference (MCS)	X-axis	*X_A_Acc1*	*X_B_Acc1*	*X_C_Acc1*
			Y-axis	*Y_A_Acc1*	*Y_B_Acc1*	*Y_C_Acc1*
			Z-axis	*Z_A_Acc1*	*Z_B_Acc1*	*Z_C_Acc1*
	02		X-axis	*X_A_Acc2*	*X_B_Acc2*	*X_C_Acc2*
			Y-axis	*Y_A_Acc2*	*Y_B_Acc2*	*Y_C_Acc2*
			Z-axis	*Z_A_Acc2*	*Z_B_Acc2*	*Z_C_Acc2*

the relevant frequencies were 31, 63, 95, 126 and 490 Hz in the X component; and 28, 57 and 86 Hz in the Y component, while for the Z component there was no interesting information.

Fig. 23 shows the maximum accelerations of each broaching tool (A, B, C) in their respective components or axes for each of the accelerometers. The maximum acceleration for each slot was taken as a reference to observe its behavior. It can be noted that there is no general trend pattern, but the sensitivity exhibited by each component and each accelerometer can be distinguished. First, the X-component has higher acceleration amplitudes than Y and Z axes, with the Z component having the lowest acceleration values of all the components. Second, in general, accelerometer 1 has higher sensitivity than accelerometer 2 except for the signals acquired from the Z-axis (Fig. 23c), where it is observed that the vibrations of Tool A, B and C of accelerometer 1 are similar in the range of 0.01 to 0.02 m/s2 and are higher than the Z component of the Tool C of accelerometer 2 (Z_C_Acc2); on the contrary, they are lower than the remaining components (Z_A_Acc2, Z_B_Acc2) by approximately one third. An inspection of all the lines representing the maximum acceleration signals shows that most of them have a negative slope to varying degrees apart from the signals in the X component of accelerometer 1. Knowing that the average wear rate (VBa) has a positive slope (Fig. 19); then, one could relate the evolution of accelerations to that of the wear rate.

Table 9 provides the labels assigned to the data obtained from the accelerometers, referring to the cutting tool and the direction in which the acceleration was measured by the accelerometer in question.

Fig. 24 shows the Pearson correlation coefficients for all acceleration signals concerning VBa. Pearson correlation coefficient is a dimensionless index, between −1 to 1, which measures the degree of linear correlation between two variables. It can be a strong direct (1), strong inverse (-1) or null (0). It is an index of easy execution and interpretation that is used in several fields of knowledge as an initial inspection technique between variables such as in engineering [28]. Overall, the best correlation found was in the Y-component of *accelerometer 1* (Fig. 24b)**,** which corresponds to the normal direction of the machined surface. A high average correlation is also evident in the X-component of accelerometer 2 (Fig. 24d) which corresponds to the radial direction of machining. In the case of the Z component, different behavior is noticed, obtaining a high average correlation only in Z_C_Acc1 and Z_C_Acc2 corresponding to the Tool C of accelerometer 1 and the Tool B of *accelerometer 2* respectively. This gives us the idea that the vibratory behavior depends a lot on the work performed by each broaching Tool, and its specific function (roughing, finishing, front face slot cutting, side face slot cutting).

A second acceleration-wear correlation analysis was carried out based on maximum values at each running frequency listed above. Figs. 25 and 26 show the best results of Pearson's correlation coefficient for *accelerometers 1* and *2* with their respective components.

According to Fig. 21, the maximum acceleration values are concentrated between the frequencies 1200 and 1400 Hz in the Y component and less than 500 Hz for the Z component; therefore. Three to four maximum characteristic process frequencies were taken according to the behavior of the signals in each axis. The correlation results of the signals obtained from *accelerometer 1* are shown in
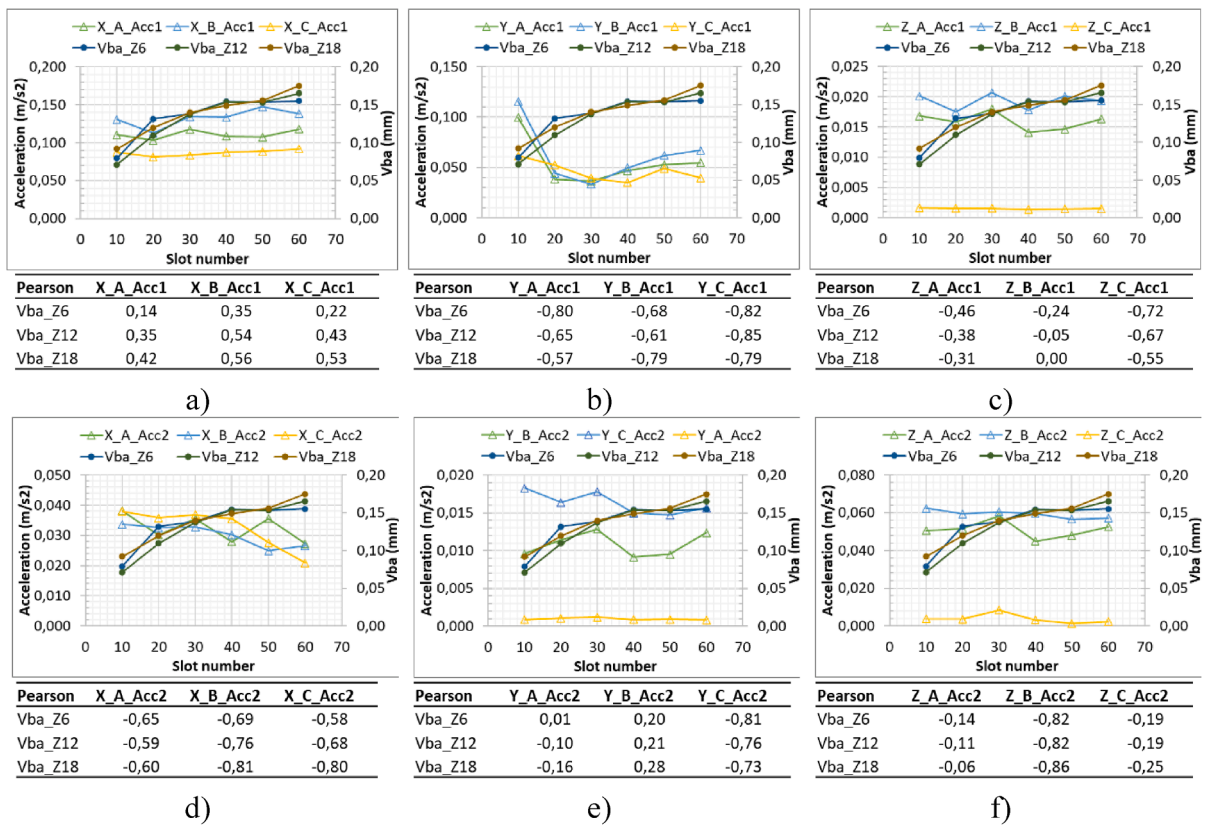
Fig. 24. Correlations between maximum acceleration per slot versus average wear VBa.

Fig. 24. In general, the existence of an inverse correlation is denoted, being this correlation stronger for the Z component and to a lesser degree for the Y-component. Differentiating between the three tool sections, Tool B obtained a higher correlation than Tool C and Tool A respectively. This degree of correlation is similarly seen in both the Y and Z axes.

From the data in Fig. 26, it can be seen that the correlations for each of the stroke or process frequencies are distinct and particular. This goes back to the results presented in Figs. 23-24 where the acquired signals are different for the 2 accelerometers. However, for certain frequencies there is a high correlation; therefore, this is a possibility to look for acceleration tracking frequencies that allow monitoring of the wear progress. An example of this can be seen in Fig. 26c, which corresponds to Tool C in the Y-component. Similarly, in Fig. 26e, a strong correlation is evident for brush B in the Z-component.

3.4. Load cell signal processing

Throughout cutting, tool edges suffer from cumulative flank wear, as a result, cutting force increases proportionally; so the measurement of cutting force is the general way of monitoring cutting tool performance. However, introducing load cells into an electromechanical broaching machine was never been done before, so it was necessary to test the load cells sensitivity. In Fig. 27 a scheme of how the cutting force is divided in the machine coordinate system is presented. With 15° counter-clockwise inclination, tool-piece engagement starts to the right.

Since the testpiece disk is inclined 15° and load cells measure in their main axis, it was necessary to make some trigonometric calculations to obtain the orthogonal cutting forces from measurements from the two load cells, shown in Fig. 27.

Fig. 28 shows how both force cells do not display the same value for broaching process, so an average of both values was calculated. Besides, the force component resulting from the non-cutting and rotating movements of the indexing table is eliminated, to only show the forces related to the metal cutting.

As can be observed in Fig. 29, cutting forces are in agreement with the calculated cutting force range values in the setup experimentation, and variations depending on the number of teeth engaged into the material (3 or 4 simultaneously) that explain the oscillation in values. Peaks are 18 or 42 depending on the teeth total number of each segment However, the value of each force shows different values during the same experimentation. This phenomenon may be due to the 15° inclination of the disk. As the workpiece is rotated, the cutting force is not applied at the same distance from the two cells, *cell 01*, receives more pressure. Since load cells are specifically designed for impact force measurements and when the teeth enter into the part, it is always broaching the tool right side that first is engaged into cutting, so load *cell 2* receives a higher impact than load *cell 01*. In Fig. 30 this circumstance is explained in
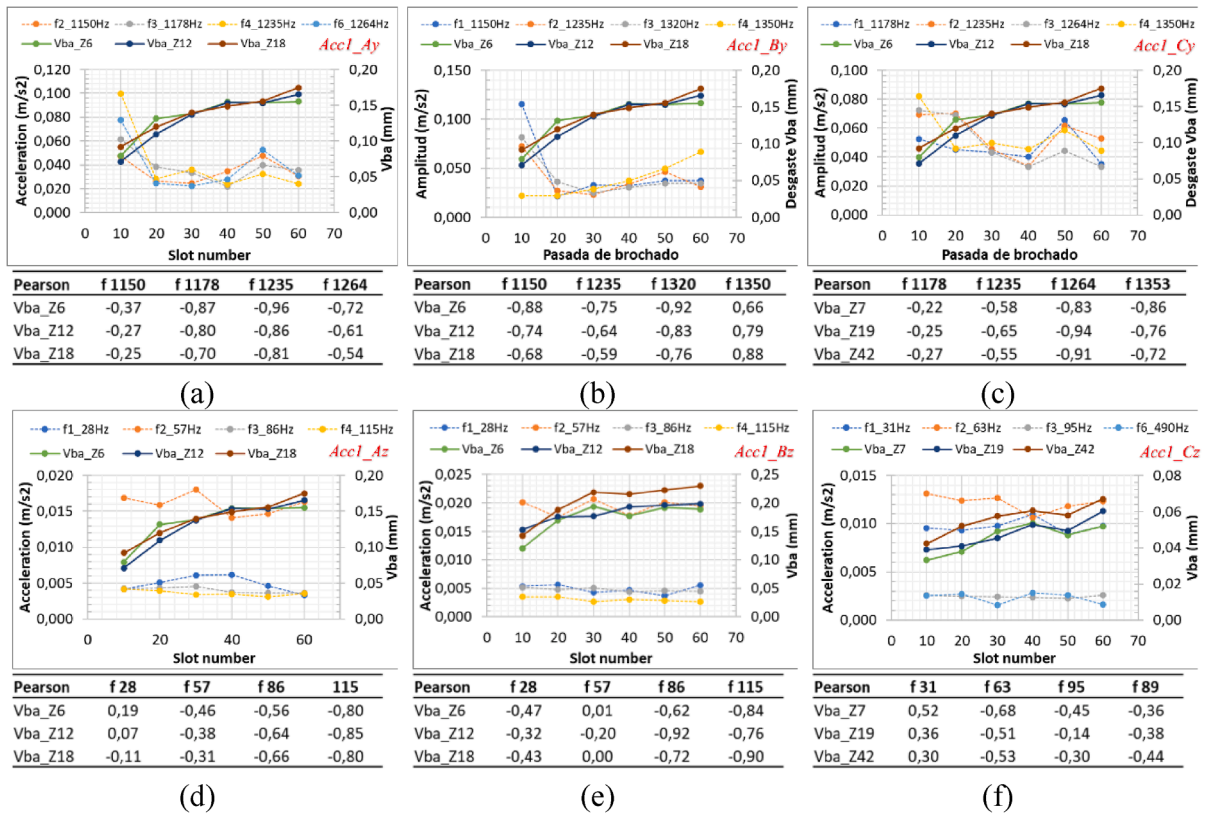
Fig. 25. Correlations between the maximum accelerations at each characteristic frequency per slot and VBa for *accelerometer 1*: **(a)** Tool A, **(b)** Tool B, **(c)** Tool C for Y component and **(d)** Tool A, **(e)** Tool B, **(f)** Tool C for Z component.

more detail.

So, during broaching process, the right tool edge zone works in harder conditions than the left side, until the last tooth left side exits from the slot. This phenomenon is observed in Fig. 31, the slope depends on the inclination angle (15° in this case). Here a zoom of each force oscillation is shown; a little peak can be due to a small backslash phenomenon. Therefore, it takes significant importance where do we place the measurement devices, since load cells only measure compression forces in the Z-axis.

4. Discussion

In this research work, broaching process monitoring was presented. Both, time and frequency domain output signals showed that there is a wide variety of methods for tool condition monitoring in broaching. Recorded signals can lead to the key characteristics of signals that can be correlated to the condition of broaching tools.

4.1. Machine internal data

The information collected by the servomotors drivers was the first choice to broaching monitoring. So, process power and torque have shown significant enough to monitor tool flank wear, presenting an acceptable linear correlation. However, it has several limitations, the first one regarding the stability of the broaching process itself; since the broaching process is fast, and the length of the first tool is small, broaching does not stabilize quickly enough to obtain data of any interest. However, once cutting becomes stable, it is possible to conclude process data. In this work, the relation between power and torque with tool wear is negative or decreasing. In other words, the more the tool wears, the lower power is consumed and the lower torque servomotors need to generate the cutting movement. The only way this can be understood is that as tooth tool tip wears, tool teeth cut less and less material reducing chip section. From a quality point of view, this means that after a certain amount of wear, the component would be out of tolerances. It remains to be analyzed in the future to determine the percentage by which the teeth are reduced and how their evolution produces a part that is out of tolerances. In industry, all people know that broaching machine and tool must be as stiff as possible, and tools as new and sharp as possible.

The carriage linear acceleration, when it goes up, has also shown interesting results when analyzed in the frequency domain. Even at the low sample frequency to record servomotor data, it was possible to achieve two harmonic frequencies of each tool segment, in addition to the tooth passing frequency. It has to be mentioned that harmonic frequencies during the experimentation were not the
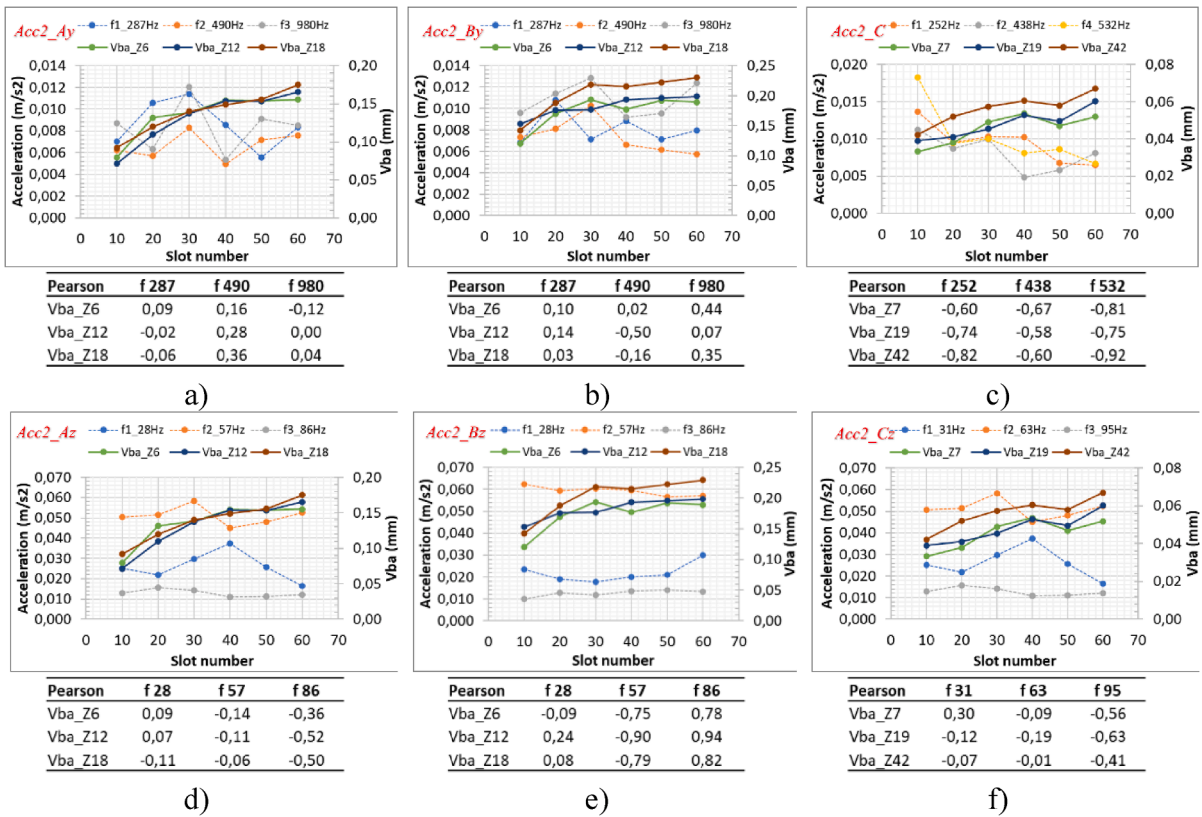
Pearson	f 287	f 490	f 980
Vba_Z6	0,09	0,16	-0,12
Vba_Z12	-0,02	0,28	0,00
Vba_Z18	-0,06	0,36	0,04

a)

Pearson	f 287	f 490	f 980
Vba_Z6	0,10	0,02	0,44
Vba_Z12	0,14	-0,50	0,07
Vba_Z18	0,03	-0,16	0,35

b)

Pearson	f 252	f 438	f 532
Vba_Z7	-0,60	-0,67	-0,81
Vba_Z19	-0,74	-0,58	-0,75
Vba_Z42	-0,82	-0,60	-0,92

c)

Pearson	f 28	f 57	f 86
Vba_Z6	0,09	-0,14	-0,36
Vba_Z12	0,07	-0,11	-0,52
Vba_Z18	-0,11	-0,06	-0,50

d)

Pearson	f 28	f 57	f 86
Vba_Z6	-0,09	-0,75	0,78
Vba_Z12	0,24	-0,90	0,94
Vba_Z18	0,08	-0,79	0,82

e)

Pearson	f 31	f 63	f 95
Vba_Z7	0,30	-0,09	-0,56
Vba_Z19	-0,12	-0,19	-0,63
Vba_Z42	-0,07	-0,01	-0,41

f)

Fig. 26. Correlations between the maximum accelerations at each characteristic frequency per slot and VBa for *accelerometer 2*: **(a)** Tool A, **(b)** Tool B, **(c)** Tool C for Y component and **(d)** Tool A, **(e)** Tool B, **(f)** Tool C for Z component.

$$F_{c,x'} = R_1 + R_2$$

$$F_{c,x'} = F_c \cdot cos\alpha$$

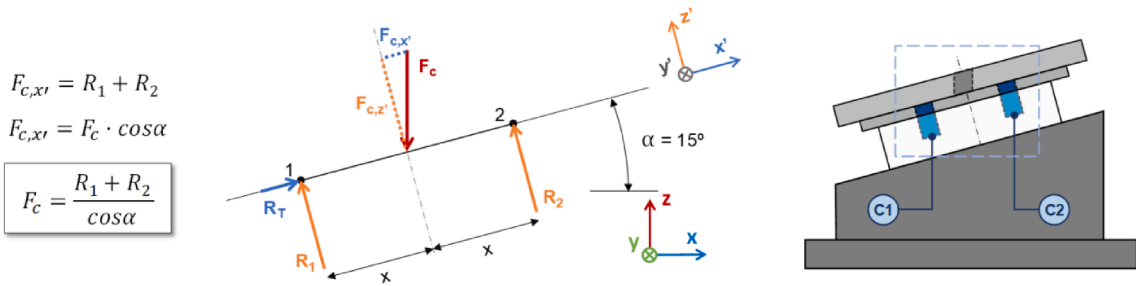$$\boxed{F_c = \frac{R_1 + R_2}{cos\alpha}}$$

$\alpha = 15°$

Fig. 27. Diagram of reactions and cutting forces of the broaching process and load cells, C1 and C2.

same due to electric noise in the data logger recording system, but compared to the cost of other acquisition systems with higher resolution and sample frequency, it was not a bad approximation. Fig. 32 shows how the tooth passing frequency (fundamental frequency) and two harmonic frequencies of both servomotors vary for each tool. It is so from Tool B, which shows that the second harmonic frequency offers the greatest relationship with tool wear growth (Fig. 33).

4.2. Accelerometers

Accelerometers offered a greater range of sampling frequencies, besides frequencies could be measured in multiple directions. Not all machine-tool directions offered good monitoring information. Thus, it was observed that the machine column and toolholder did not offer relevant information, and only the moving part of the machine, the carriage and rotary table where the testing part is clamped, gave us useful tool condition information. The accelerometer raw signals did not offer much information; however, it can detect unexpected interferences between tool and machine, which are represented as high peaks in the time domain.

Analyzing accelerations, Fig. 23 showed a high inverse correlation between Y-axis acceleration with wear, and acceleration in the X-axis with wear for accelerometers 1 and 2 respectively. In the first case, it corresponds to the normal direction to machined surfaces
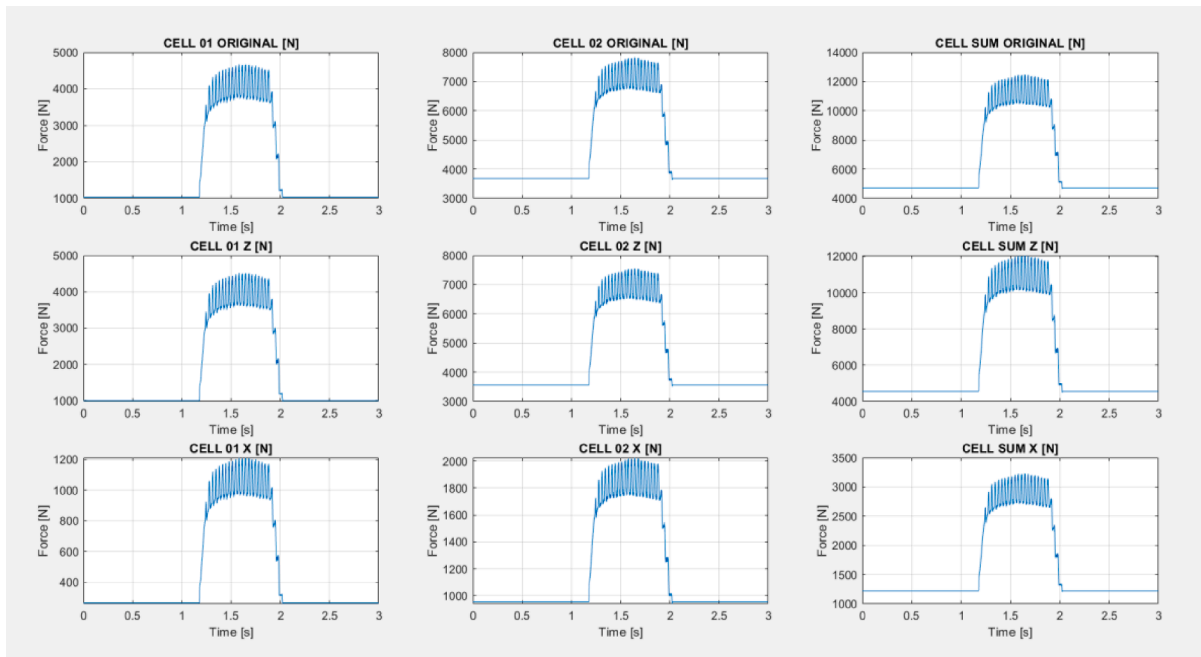
Fig. 28. Cutting force results for Tool B. The X component is absorbed by rotary table carriage guides.

and column, which means that this signal would be related to process vibrations (even onset of chatter). In reference to the inverse correlation, it coincides with several studies showing a decrease in process vibration as the flank wear increases (due to the so-called process damping). Many studies focused on turning and milling processes where cutting is continuous in time, cutting speed is relatively higher and cutting width is small; unlike the broaching process, between slots there is a dead time or lapse when broach interaction is interrupted until the next cycle, the cutting speed is lower, and cutting edge width large. However, studies are reporting that tool flank wear plays an important positive damping role in vibration at both high and low speeds, and some reported that cutting edge width may be independent of this damping [27,29]. Chatter in broaching can be very interesting, and it will need further investigations.

In the second case where the vibration of *accelerometer 2* in X-axis has an inverse correlation with wear, it could also complement case 1 or provide information about lateral vibrations.

Finally, process damping is mainly attributed to the cutting-edge microgeometry. In the worn-out zone (Fig. 13), the tool rubbing due to natural wear could have influenced the reduction in the vibration amplitude.

In the analysis of tooth passing frequency (Fig. 25) concerning vibration, two situations stand out. First, the inverse correlation between wear and acceleration in the Y-axis is confirmed with small differences in behavior between the three broaches. To correspond to what was said above, this may be due to the tool edge radius which is different between Tool A, B and C. The second aspect is that small gaps were found in the frequencies of each slot. This may be due to the process dynamics, causing small amplification or damping in the acceleration of the next slot.

Vibrations signals, especially in the Y-axis, can give information about the progress of tool wear as well as process stability, which needs to be further investigated. The vibration signal in X on the column (*accelerometer 2*) gives a high inverse correlation, which can give valuable process information as well. Finally, acceleration signals are feasible for monitoring the process and predicting tool wear increment.

4.3. Load cells

Load cells, like accelerometers, are a source of a lot of information, because the high sampling rate allows them to capture any anomaly that occurs during the cutting process. In this case, it allows to understand how the piece/table inclination affects. Fig. 31 shows how, as a tooth enters, the force gradually increases, and when the stability zone should be reached, there is a little disturbance with a negative peak. This phenomenon does not occur systematically, but rather randomly. Signals matching machine tool frequencies must be disregarded because the amplitudes are affected by dynamic amplification [26,27].

Aircraft engine components are known for their high quality and cost, one of them can reach around 75,000–100,000€. Therefore, predicting tool failure and avoiding wrong parts is a considerable saving. Furthermore, with proper monitoring system it is possible to rescue the tool and re-sharpen (and re-shape) it for re-use. Broaching tools are around 5000 € (in 2022) for the roughing set alone. Compared to these numbers, a simple monitoring system is very cost-effective to implement on the machine. For example, collect the motor driver signals does not require for any device, so do not have any additional cost. Implementing accelerometers (700 €) or load
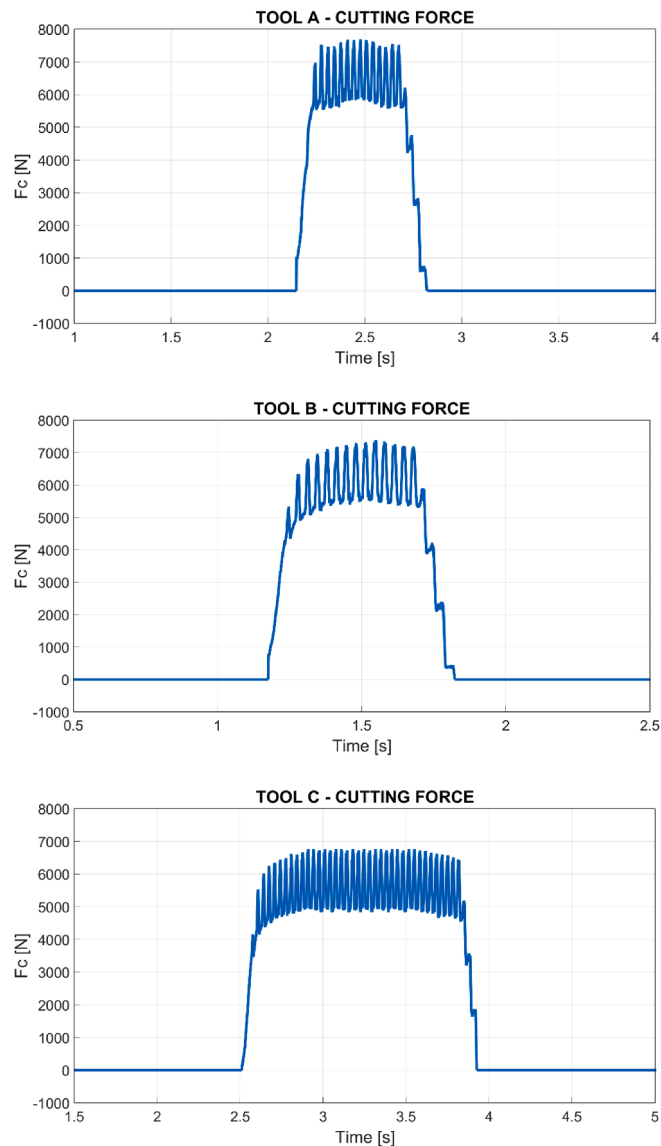
Fig. 29. Coated (Tool A and B) with 18 peaks, and uncoated cutting tool (Tool C) with 42 peaks, force in Z-axis. Three teeth are always in cut, sometimes four, due to disk thickness, see Eqs. (5)–(7).

cells (400 €) requires a higher investment, because a signal acquisition system is also necessary, which ranges from 3000 to 10,000 €, depending on the model. To these raw values, it would be necessary to add the hours of calibration and testing. But one or two pieces saved and ready to fly are equivalent to the investment in a monitoring system, by far.

Once the capabilities of the monitoring methods available are better understood, they could be implemented in a closed-loop system to determine whether the tool must be resharpened. Fig. 34 shows a possible application in a real industry, in this case, to allow a replacement policy with broaching tools. Broaching tools can be re-sharpened, from 4 to 8 times.

5. Conclusions

In this paper, the data recording system of an electrically-driven broaching bench is presented. This work aims to obtain a reliable way of extracting data from broaching and uploading it to the cloud, in an organized way to be useful for future applications based on a machine learning approach, where cutting process data and part quality measurements could be merged. The main conclusions derived from this work are cited:

- Regarding the motor drivers, only the power and torque feedback signals can monitor the broaching process in the time domain. In addition, to do this efficiently, the cutting process must reach a stable condition; otherwise, the values do not show a clear trend.
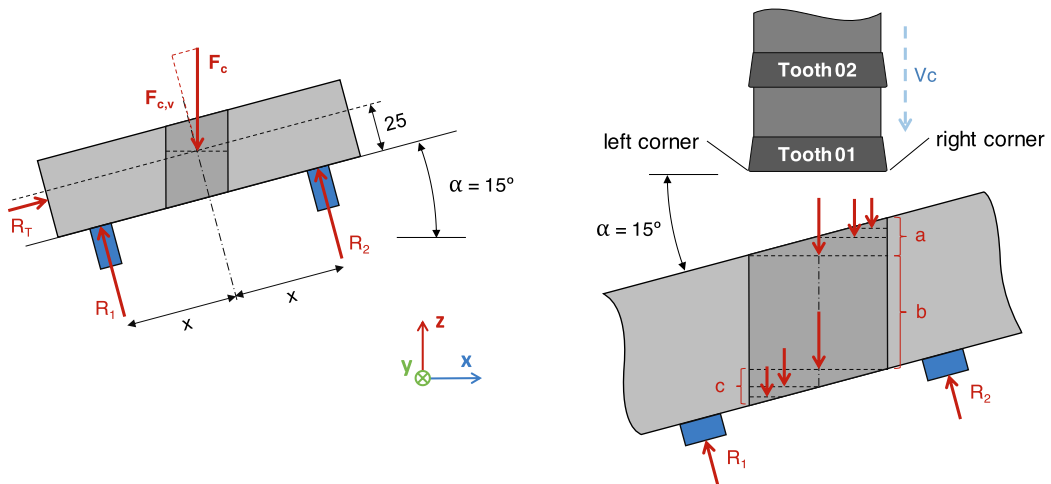
Fig. 30. Scheme of the cutting force during the entry of the tool into the workpiece. Cutting edge right corner is the first engaging into disk.
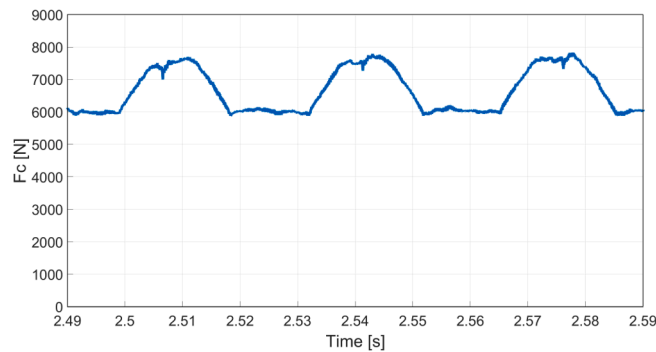

Fig. 31. Evolution of the cutting force during the entry of the teeth. Slope depends on the inclination angle, 15° in this case.

- Servomotor electrical current does not offer any information either from the cutting process or from cutting tool performance.
- The linear acceleration values extracted from the drivers are capable of sensing some degree of variation in the frequency domain. However, due to electrical noise and very small sample frequency, only two natural frequencies were recorded, with the second frequency showing the highest correlation with tool wear.
- Accelerometer signals give information related to broaching tool wear. In particular, the highest sensitivity was obtained for the X component for both *accelerometers 1* and *accelerometer 2*, with slight differences in behavior between broach segments A and B.
- Notable differences and correlation results were obtained for the Y component of the accelerometer signals. For *accelerometer 1* there were very high correlations for Tools A and B and medium correlation for C. On the other hand, based on the results obtained, the low correlation obtained in the Y component of all broaching tools is due to the high noise in the signals of this component.
- The maximum frequencies per slot can indicate worm-out tools. This information is very well complemented by the analysis of the tooth passing frequency.
- Accelerometers placed on the machine rotary table have better sensitivity than accelerometers placed on the machine column.
- According to the inverse correlation results for most frequencies, this indicates that the acceleration is high at the beginning of broaching and decreases as the broach wears progressively. In this particular case, it is reflected in the initial and final machined slots, and the main cause can be the increased damping of the process due to tool wear.
- In this work, load cells were only used to confirm that the cutting force was inside a secure range for the safety of the machine, but it offers interesting values about the performance of each cutting tooth, so it is possible to perceive any variation in the geometry of each of them.
- Besides, load cells were also valuable resources to understand how the multiple edge cutting tool works when the piece is inclined.

Finally, the monitoring system is able for industrial production, in which internal motor signals on one hand, and not too many additional sensors are a reasonable solution. However, there is still further work to do:
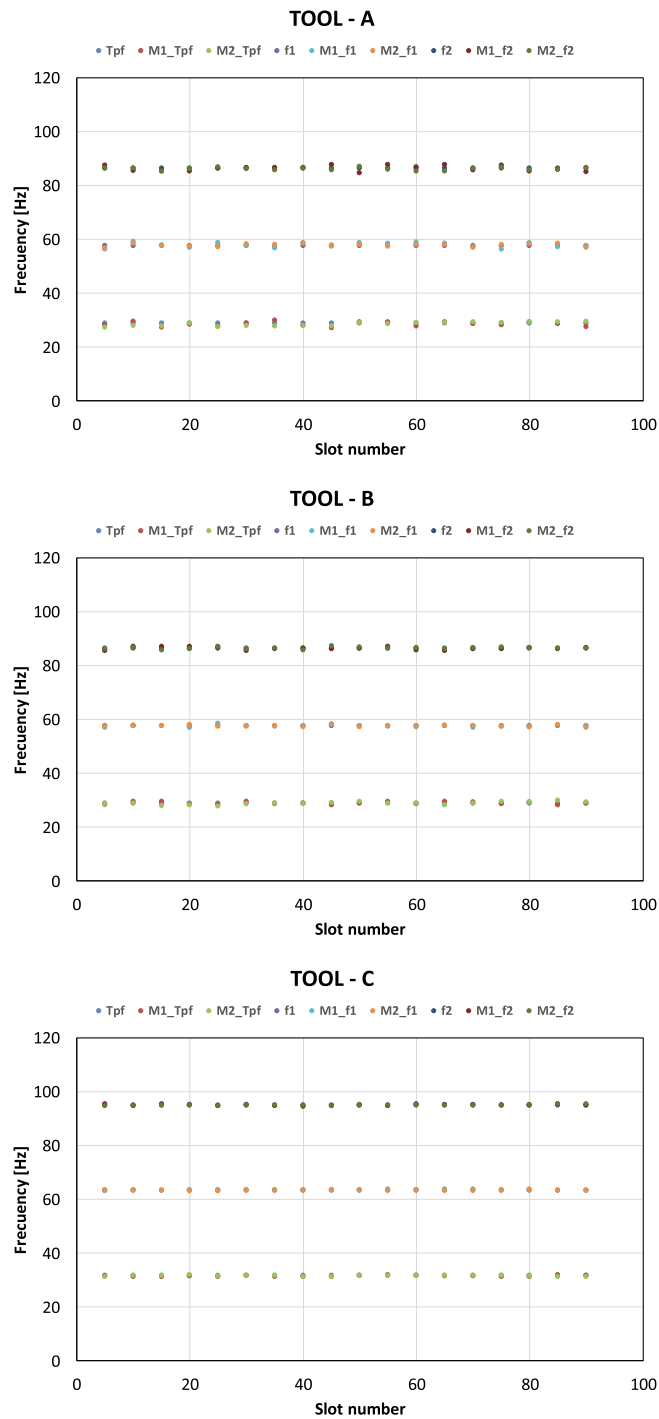
Fig. 32. Tooth passing frequency (fundamental frequency) and two harmonic frequencies measurement of both servomotors difference, for each tool along testing.

- In our tests, not all broaches reach their end of life, none reaches 0.3 mm of flank wear. Further machining should be done with Tool C, to check that process signals evolve in the same way as Tool B.
- Rubbing effect at tool tip can be studied using ideas coming from burnishing processes [30], because slot internal surfaces can be affected regarding residual stresses.
- The load cells were only used to check force maximum magnitude. In future tests, it is planned to check how the cutting force evolves as the broaching tool wears, based on analyzing load cell signatures.
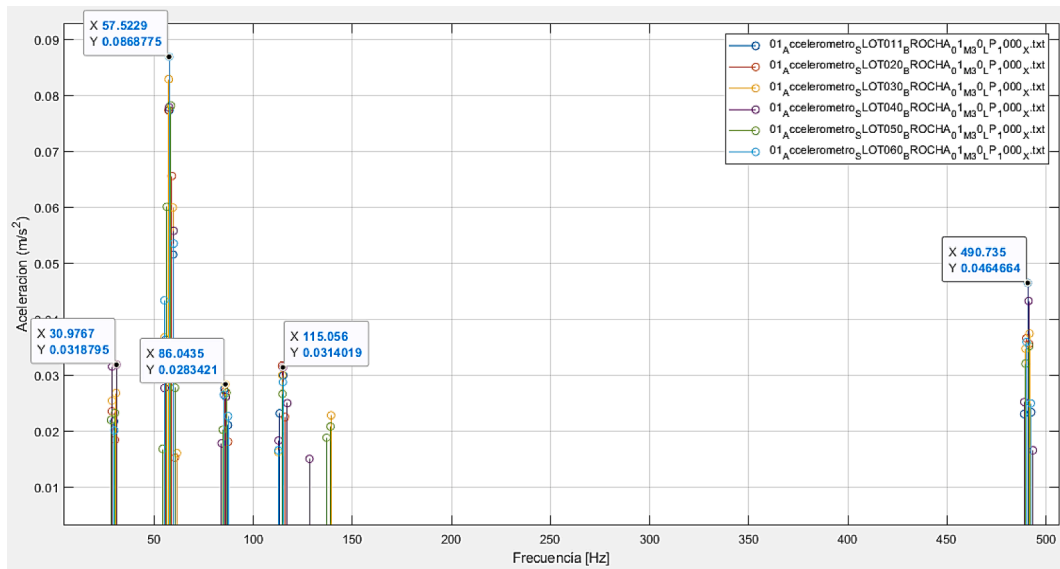
Fig. 33. Plotting of 30 maximum acceleration points of Tool A in the Y-axis for slots 10, 20, 30, 40, 50, 50 and 60.
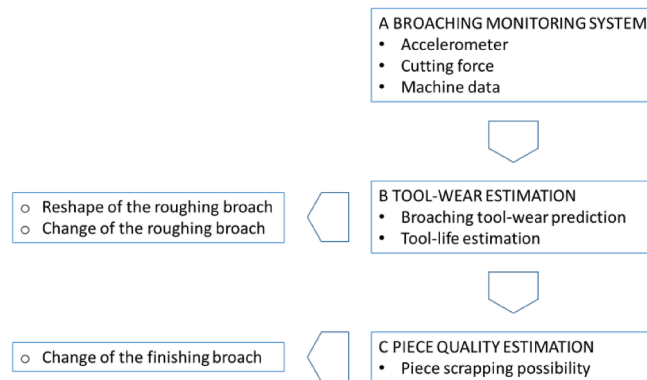

Fig. 34. Flowchart to avoid waste of time and money in broaching of turbine critical systems.

- Regarding the accelerometers, it would be interesting to carry out further tests by moving the position of *accelerometer 01* along the machine column. To see if signals with a higher correlation with the wear of the process are captured in another position.
- Broaching tool skew angle was cero, but in future, some tools can be manufacture and tested with a *skew angle* similar to the inclination angle (15°), to have a constant chip section during one tooth edge cutting. This can help to avoid edge chipping on the teeth right side due to hits at tool engagement.

Funding

Declaration of Competing Interest

The authors declare that they have no known competing financial interests or personal relationships that could have appeared to influence the work reported in this paper.

Acknowledgments

All authors have read and agreed to the published version of the manuscript.

References

[1] P.J. Arrazola, J. Rech, R. M'Saoubi, D. Axinte, Broaching: Cutting tools and machine tools for manufacturing high quality features in components, CIRP Ann. 69 (2) (2020) 554–577, https://doi.org/10.1016/j.cirp.2020.05.010.

[2] D. Fabre, C. Bonnet, J. Rech, T. Mabrouki, Optimization of surface roughness in broaching, CIRP J. Manuf. Sci. Technol. 18 (2017) 115–127, https://doi.org/10.1016/j.cirpj.2016.10.006.

[3] A.P. Stephens, Broaching Machines (1873) 1–2.

[4] P. Gilormini, E. Felder, L. Tronchet, F. Leroy, F. Le Maitre, A comparative analysis of three machining processes: broaching, tapping and slotting, CIRP Ann. - Manuf. Technol. 33 (1) (1984) 19–22, https://doi.org/10.1016/S0007-8506(07)61371-7.

[5] L. Vijayaraghavan, R. Krishnamurthy, H. Chandrasekaran, Evaluation of stress and displacement of tool and workpiece on broaching, Int. J. Mach. Tool Design Res. 21 (1981) 263–270.

[6] V. Sajeev, L. Vijayaraghavan, U.R.K. Rao, Effect of tool-work deflections on the shape of a broached hole, Int. J. Mech. Eng. Educ. 28 (1) (2000) 88–92, https://doi.org/10.7227/IJMEE.28.1.7.

[7] V. Sajeev, L. Vijayaraghavan, U.R.K. Rao, An analysis of the effects of burnishing in internal broaching, Int. J. Mech. Eng. Educ. 28 (2) (2000) 163–173, https://doi.org/10.7227/IJMEE.28.2.5.

[8] T. Bergs, G. Smeets, M. Seimann, B. Doebbeler, A. Klink, F. Klocke, Surface integrity and economical assessment of alternative manufactured profiled grooves in a nickel-based alloy, Procedia Manuf. 18 (2018) 112–119, https://doi.org/10.1016/j.promfg.2018.11.015.

[9] A. Hosseini, On the quality and integrity of broached surfaces, Int. J. Adv. Manuf. Technol. 102 (1-4) (2019) 95–103, https://doi.org/10.1007/s00170-018-3132-1.

[10] R. Ahmad, H. Al-Rawashdeh, A.O. Hasan, Optimization of keyway broach design, J. Fail. Anal. Prev. 19 (3) (2019) 688–697, https://doi.org/10.1007/s11668-019-00647-5.

[11] A. Hosseini, H.A. Kishawy, On the optimized design of broaching tools, J. Manuf. Sci. Eng. Trans. ASME 136 (2014) 1–10, https://doi.org/10.1115/1.4025415.

[12] F. Klocke, B. Döbbeler, M. Seimann, Dry broaching using carbon free steel as tool material, Procedia CIRP 46 (2016) 496–499, https://doi.org/10.1016/j.procir.2016.04.076.

[13] F. Klocke, P. Vogtel, S. Gierlings, D. Lung, D. Veselovac, Broaching of Inconel 718 with cemented carbide, Prod. Eng. 7 (6) (2013) 593–600, https://doi.org/10.1007/s11740-013-0483-1.

[14] P. Vogtel, F. Klocke, H. Puls, S. Buchkremer, D. Lung, Modelling of process forces in broaching Inconel 718, Procedia CIRP 8 (2013) 409–414, https://doi.org/10.1016/j.procir.2013.06.125.

[15] M. Seimann, B. Peng, A. Fischersworring-Bunk, S. Rauch, F. Klocke, B. Döbbeler, Model-based analysis in finish broaching of Inconel 718, Int. J. Adv. Manuf. Technol. 97 (9-12) (2018) 3751–3760, https://doi.org/10.1007/s00170-018-2221-5.

[16] C. Legrand, G. Fromentin, G. Poulachon, R. Chatain, M. Rancic, A geometrical and mechanistic generalized model for complex shape broaching of super alloy, Procedia CIRP 82 (2019) 461–466, https://doi.org/10.1016/j.procir.2019.04.042.

[17] E. Özlü, A. Ebrahimi Araghizad, E. Budak, Broaching tool design through force modelling and process simulation, CIRP Ann. 69 (1) (2020) 53–56, https://doi.org/10.1016/j.cirp.2020.04.035.

[18] E. Budak, Broaching process monitoring, in: Proceedings of the Proceedings of Third International Conference on Metal Cutting and High Speed Machining, 2001, pp. 251–260.

[19] A. Fernández-Valdivielso, L.N. López de Lacalle, P. Fernández-Lucio, H. González, Turning of Austempered Ductile Iron with ceramic tools, Proc. Inst. Mech. Eng. Part B J. Eng. Manuf. 235 (3) (2021) 484–493, https://doi.org/10.1177/0954405420957154.

[20] D.A. Axinte, N. Gindy, Tool condition monitoring in broaching, Wear 254 (2003) 370–382, https://doi.org/10.1016/S0043-1648(03)00003-6.

[21] D. Axinte, F. Boud, J. Penny, N. Gindy, D.J. Williams, Broaching of Ti-6-4 - Detection of workpiece surface anomalies on dovetail slots through process monitoring, CIRP Ann. - Manuf. Technol. 54 (1) (2005) 87–90, https://doi.org/10.1016/S0007-8506(07)60056-0.

[22] R. Stoney, T. Pullen, B. Aldwell, S. Gierlings, M. Brockmann, D. Geraghty, D. Veselovac, F. Klocke, G.E.O. Donnell, Observations of surface acoustic wave strain and resistive strain measurements on broaching tools for process monitoring, Procedia CIRP 14 (2014) 66–71, https://doi.org/10.1016/j.procir.2014.03.024.

[23] F. Klocke, S. Gierlings, O. Adams, T. Auerbach, S. Kamps, D. Veselovac, M. Eckstein, A. Kirchheim, M. Blattner, R. Thiel, D. Kohler, New concepts of force measurement systems for specific machining processes in aeronautic industry, Procedia CIRP 1 (2012) 552–557, https://doi.org/10.1016/j.procir.2012.04.098.

[24] R.E. Schafrik, D.D. Ward, J.R. Groh, Application of alloy 718 in GE aircraft engines: past, present and next five years, Proc. Int. Symp. Superalloys Var. Deriv. 1 (2001) 1–11, https://doi.org/10.7449/2001/superalloys_2001_1_11.

[25] A.I. Fernández-Abia, J. Barreiro, L.N. López de Lacalle, S. Martínez-Pellitero, Behavior of austenitic stainless steels at high speed turning using specific force coefficients, Int. J. Adv. Manuf. Technol. 62 (2012) 505–515, https://doi.org/10.1007/s00170-011-3846-9.

[26] L.N.L.d. Lacalle, A. Lamikiz, J.A. Sánchez, I.F.d. Bustos, Recording of real cutting forces along the milling of complex parts, Mechatronics 16 (1) (2006) 21–32, https://doi.org/10.1016/j.mechatronics.2005.09.001.

[27] L.N.L. LopezdeLacalle, A. Lamikiz, J.A. Sanchez, I.F. FernandezdeBustos, Simultaneous measurement of forces and machine tool position for diagnostic of machining tests, IEEE Trans. Instrum. Meas. 54 (6) (2005) 2329–2335, https://doi.org/10.1109/TIM.2005.858535.

[28] Pearson's Correlation Coefficient. In *Encyclopedia of Public Health*; Kirch, W., Ed.; Springer Netherlands: Dordrecht, 2008; pp. 1090–1091 ISBN 978-1-4020-5614-7.

[29] C.M. Taylor, N.D. Sims, S. Turner, Process damping and cutting tool geometry in machining, IOP Conf. Ser. Mater. Sci. Eng. 26 (2011), https://doi.org/10.1088/1757-899X/26/1/012009.

[30] Estudio de la influencia de la presión del bruñido hidrostático por bola en la rugosidad superficial del INCONEL® 718 y del TI6AL4V (Study of the influence of hydrostatic ball burnishing pressure on the surface roughness of the IN718 and Ti6Al4V), P. Fernández-Lucio, G. Gómez-escudero, A. del Olmo, F. Marin, A. Rodríguez, L.N. López de Lacalle, *Revista Iberoamericana de Ingeniería Mecánica.* **2021**, 25, 2, 21–28.